Electronic Research Archive

https://www.aimspress.com/journal/era

ERA, 33(2): 907–930.
DOI: 10.3934/era.2025041
Received: 16 December 2024
Revised: 24 January 2025
Accepted: 11 February 2025
Published: 19 February 2025

Research article

The nonlinear observer-based fault diagnosis method for the high altitude airship

Jichen Hu[1], **Ming Zhu**[2] **and Tian Chen**[2,*]

[1] School of Aeronautic Science and Engineering, Beihang University, Beijing 100191, China
[2] Institute of Unmanned System, Beihang University, Beijing 100191, China

* **Correspondence:** Email: chen_tian@ buaa.edu.cn.

Abstract: We investigated an observer-based fault diagnosis method for the high altitude airship (HAA). The nonlinear kinematics and dynamics model, which considers model uncertainties and external disturbances, were obtained. The nonliear portion of the model was re-expressed to the linear parameter varying frame mathematically with an auxiliary design. Subsequently, in order to realize fault detection, isolation, and reconstruction, diverse types of robust were observers designed, respectively. Furthermore, all these mentioned observers were achieved via the linear matrix inequation framework. The effectiveness of the proposed method was verified by different fault cases in an HAA simulation system.

Keywords: the high altitude airship; fault diagnosis; nonlinear system; robust observer; linear parameter varying

1. Introduction

The high altitude airship (HAA) is a controllable unmanned aerostat that has a high cruise altitude of more than 18 kilometers. Compared to other aircraft, the ability of flight area station keeping and long endurance make it have prospective applications in widespread fields such as high altitude scientific observation, area gazed surveillance, and communication link relay support [1]. Over the past decade, the research on the HAA expanded greatly and achieved in some results in motion and attitude control [2–4]. Nevertheless, these studies of control leave out the failure occurrence, which is inevitable in long-duration flights that may exceed several months. The control system, which comprises sensors, actuators, and the controller, is a crucial subsystem of an HAA. The fault represents the contradiction between actual and expected system state. When the unknown fault occurs in either component, it leads to a complex effect on the control system to cause the performance decline of the control, or even out of control. The impact can be avoided by timely and accurate fault diagnosis (FD) technology. As

a consequence, to ensure the reliability and stability of the control system, the FD function is essential to implement.

Generally, the complete FD scheme is supposed to reach functions that confirm the occurrence of faults, identify the location of the faulty component, and describe the time-varying size of the unknown fault. Namely, they are fault detection, isolation, and estimation, respectively. The result of fault detection will provide an alarm when any fault of the control system occurs. Some other details of the unknown fault can be the input of a designed controller, which can compensate for the effect caused by the fault. It is a precondition for an investigative route of the active fault-tolerant control (FTC) technology.

With the development of control theory and computer technique, diverse FD schemes have been proposed. In aerospace engineering, the hardware redundancy method has been applied commonly for some devices such as inertial navigation system and actuators. The HAA is analogous to the spacecraft, in that the carrying capacity and the bandwidth of the telemetry command link are limited. Employing multiple pieces of equipment is not applicable, particularly for the actuators. The analytical redundancy scheme is proposed to substitute the hardware redundancy. Its advantage is that relationships between system inputs and outputs is modeled mathematically. There are two major methods of the analytical redundancy scheme: Data-based and model-based. The data-based method focuses on analyzing data from the measured system state to achieve the purpose of FD, which has got some practical results, such as statistics-based [5] and machine learning [6]. The model-based method emphasizes the establishment of a mathematically precise model of the system. The residual of the system and mathematical model outputs is evaluated to achieve FD [7]. In this scheme, the study of the observer-based method is widely developed [8, 9] and is applied in unmanned aerial vehicle (UAV) and satellite systems [10–12]. It is challenging to design a nonlinear observer under unknown external disturbances and system uncertainty [13]. Some researchers linearzed or partially linearized the nonlinear system to design observers [14–16]. Moreover, adaptive observer [17] methods are used to approximate the nonlinear functions in the system. Two types of observers are designed in [18] for known and unknown dynamic faults entering the system via nonlinear functions. The interval observer technique and developed methods are utilized to detect and isolate faults with an esitmation interval in discrete-time systems [19, 20]. For fault reconstruction, the effectiveness of the silding-model observer (SMO) method is verified in the Takagi-Sugeno model [21] and FD in linear system [22]. Additionally, an extended SMO fix-time is applied in the FTC of an unmanned airship [23], and the polytopic sliding mode observer is developed for fault detection and reconstruction in descriptor linear systems [24].

When fault exists in the system, choosing a suitable residual evaluation function can reflect the state of a real system effectively. In most studies, the L_2-norm of the output error is employed as the residual evaluation. However, dimensions of state vary greatly, such as position state and angular velocity. Hence, residual reflected in certain state quantities can be masked by measurement noise or system disturbance.

To address the FD for the HAA, we propose an integrated $\mathcal{H}_\infty$ nonlinear observer-based method. With the aim of fault detection, isolation, and reconstruction, appropriate observer types are adopted correspondingly. The state estimation error dynamics is converted to a novel linear parameter varying (LPV) structure with mathematical inferences to cope with system nonlinearity. Nonlinear observations are achieved by linear matrix inequation (LMI) to ensure the convergence of state

estimation error and robustness to extra disturbance and system uncertainty. A novel residual evaluation function is proposed to develop the feature extraction. Some real typical failure cases are provided for an HAA flight simulation system to demonstrate the effectiveness of the proposed method. The main contribution of this work is summarized as follows:

1) A feasible and compositive nonlinear observer-based FD method is applied to the HAA, and the applicability of the designed observer depends on the sub-task of the FD.

2) The reformulated LPV form, which is directly inferred from the state estimation error dynamics, provides less conservative Lipschitz conditions without additional computational complexity.

3) Considering the residual feature is hidden by the disturbance and measurement noise, the residual evaluation is developed and improves effectiveness.

The rest of this paper is organized as follows: In Section 2, we provide the HAA modeling and FD problem description. The design of nonlinear observers is presented in Section 3 in detail as the major results. In Section 4, some FD cases are in the HAA simulation system to illustrate the practicability of the proposed method. Finally, our work of this paper is summarized, and the conclusions are given in Section 5.

2. Preliminaries

2.1. The modeling of the HAA

The typical structure of an HAA studied in this paper is shown in Figure 1. The main structure, which provides buoyancy, is an overpressure envelope symmetric to the longitudinal axis. Empennages provide the static stability. The avionics gondola are installed under the envelope. Actuators are installed on the envelope to respond to the controller output and produce control force and moment. The overpressure envelope is considered a rigid body.

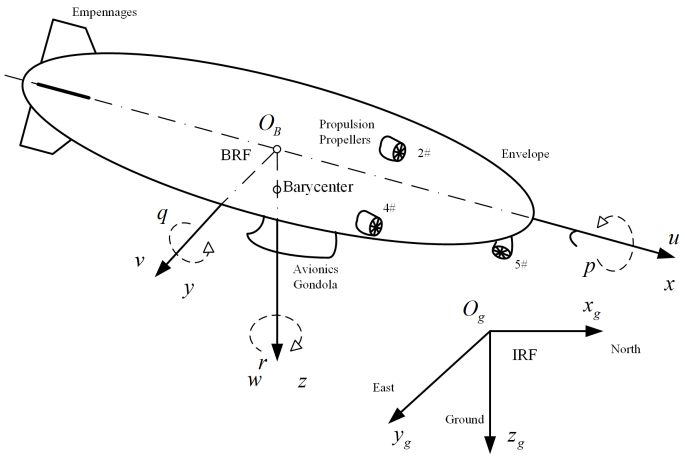

Figure 1. The structure of the HAA.

Therefore, the translational and the rotational motion are described by a 6 degrees of freedom (DOF) nonlinear dynamic model derived from Newton-Euler law. The velocity $\mathbf{v} = [u, v, w]^T$ and angular

velocity $\boldsymbol{\omega} = [p, q, r]^T$ are defined in the body reference frame (BRF) whose origin O_B is the centroid of the HAA. The 6-DOF dynamic model is presented as:

$$\mathbf{M}\begin{bmatrix} \dot{\mathbf{v}} \\ \dot{\boldsymbol{\omega}} \end{bmatrix} + \mathbf{G}(\mathbf{v}, \boldsymbol{\omega}) = \boldsymbol{\tau}_A + \boldsymbol{\tau}_B + \boldsymbol{\tau}_P \tag{2.1}$$

with

$$\mathbf{M} = \begin{bmatrix} (m_0 + m_a)\boldsymbol{I} & -m_0 \boldsymbol{c}_G^{\times} \\ m_0 \boldsymbol{c}_G^{\times} & \boldsymbol{I}_0 + \boldsymbol{I}_a \end{bmatrix} \tag{2.2}$$

and

$$\mathbf{G}(\mathbf{v}, \boldsymbol{\omega}) = \begin{bmatrix} (m_0 + m_a)\boldsymbol{I} \cdot \boldsymbol{\omega}^{\times} \cdot \mathbf{v} + m_0 \boldsymbol{I} \cdot \boldsymbol{\omega}^{\times}(\boldsymbol{\omega}^{\times} \cdot \boldsymbol{v}_G) \\ \boldsymbol{\omega}^{\times}(\boldsymbol{I}_0 \boldsymbol{\omega}) + m_0 \boldsymbol{I} \cdot \boldsymbol{v}_G^{\times}(\boldsymbol{\omega}^{\times} \cdot \mathbf{v}) \end{bmatrix} \tag{2.3}$$

where $\boldsymbol{I}$ denotes the identity matrix with appropriate dimension. m_0, m_a, $\boldsymbol{I}_0$, and $\boldsymbol{I}_a$ denote the mass, additional mass, inertia, and additional inertia, respectivly. $\boldsymbol{v}_G$ denotes the barycenter vector in the BRF. The notation $\boldsymbol{a}^{\times}$ denotes the skew-symmetric matrix for vector $\boldsymbol{a}$. $\boldsymbol{\tau}_A$ presents the aerodynamic force and torque vector. $\boldsymbol{\tau}_B$ presents the resultant force and torque vector of the gravity and buoyancy. $\boldsymbol{\tau}_P = \begin{bmatrix} \boldsymbol{F}_P \\ \boldsymbol{M}_P \end{bmatrix}$ presents the thrust $\boldsymbol{F}_P$ and rotation torque $\boldsymbol{M}_P$ produced by the propulsion actuators.

When the dynamics are obtained, the HAA position $\mathbf{P} = [x_g, y_g, z_g]^T$ and attitude angle $\boldsymbol{\Omega} = [\phi, \theta, \psi]^T$ in the inertial reference frame (IRF),whose origin O_g is the point on the ground, describe the HAA kinematics, which is given by

$$\begin{bmatrix} \dot{\mathbf{P}} \\ \dot{\boldsymbol{\Omega}} \end{bmatrix} = \begin{bmatrix} \mathbf{R}_{\mathrm{v}} & \\ & \mathbf{R}_{\Omega} \end{bmatrix} \begin{bmatrix} \mathbf{v} \\ \boldsymbol{\omega} \end{bmatrix} \tag{2.4}$$

with rotation matrices $\mathbf{R}_{\mathrm{v}} = \begin{bmatrix} \mathbf{c}_\theta \mathbf{c}_\psi & \mathbf{s}_\theta \mathbf{c}_\psi \mathbf{s}_\phi - \mathbf{s}_\psi \mathbf{c}_\phi & \mathbf{s}_\theta \mathbf{c}_\psi \mathbf{c}_\phi + \mathbf{s}_\psi \mathbf{s}_\phi \\ \mathbf{c}_\theta \mathbf{s}_\psi & \mathbf{s}_\theta \mathbf{s}_\psi \mathbf{s}_\phi + \mathbf{c}_\psi \mathbf{c}_\phi & \mathbf{s}_\theta \mathbf{s}_\psi \mathbf{c}_\phi - \mathbf{c}_\psi \mathbf{s}_\phi \\ -\mathbf{s}_\theta & \mathbf{c}_\theta \mathbf{s}_\phi & \mathbf{c}_\theta \mathbf{c}_\phi \end{bmatrix}$ and $\mathbf{R}_{\Omega} = \begin{bmatrix} 1 & \mathbf{s}_\phi \tan\theta & \mathbf{c}_\phi \tan\theta \\ 0 & \mathbf{c}_\phi & -\mathbf{s}_\phi \\ 0 & \frac{\mathbf{s}_\phi}{\mathbf{c}_\theta} & \frac{\mathbf{c}_\phi}{\mathbf{c}_\theta} \end{bmatrix}$,

where $\mathbf{s}_{(\cdot)} \triangleq \sin(\cdot)$ and $\mathbf{c}_{(\cdot)} \triangleq \cos(\cdot)$.

2.2. Problem description

Let the state vector $\boldsymbol{x} = \begin{bmatrix} \mathbf{P} \\ \boldsymbol{\Omega} \\ \mathbf{v} \\ \boldsymbol{\omega} \end{bmatrix} \in \mathbb{R}^n$, and the HAA model is presented as a class of a nonlinear system form as:

$$\dot{\boldsymbol{x}} = \boldsymbol{G}(\boldsymbol{x}) + \boldsymbol{B}\boldsymbol{u} + \boldsymbol{\eta} \tag{2.5}$$

where $\boldsymbol{G}(\boldsymbol{x}) = \begin{bmatrix} \mathbf{R}_{\mathrm{v}}\mathbf{v} \\ \mathbf{R}_{\Omega}\boldsymbol{\omega} \\ \mathbf{M}^{-1}(\boldsymbol{\tau}_A + \boldsymbol{\tau}_B - \mathbf{G}(\mathbf{v}, \boldsymbol{\omega})) \end{bmatrix} \in \mathbb{R}^n$ is the known nonlinear function. Due to the low dynamic characteristics of the HAA, nonlinear function $\boldsymbol{G}(\cdot)$ is Lipschitz with a positive constant α so that $\|\boldsymbol{G}(\boldsymbol{x}_1) - \boldsymbol{G}(\boldsymbol{x}_2)\| \leq \alpha \|\boldsymbol{x}_1 - \boldsymbol{x}_2\|$ for two vectors $\boldsymbol{x}_1$ and $\boldsymbol{x}_2$. From dynamics (2.1) and kinematic (2.4), $\boldsymbol{B}\boldsymbol{u} = \begin{bmatrix} \mathbf{0} \\ \mathbf{M}^{-1}\boldsymbol{\tau}_P \end{bmatrix}$ is obtained, where $\boldsymbol{u} \in \mathbb{R}^q$ is the system input and $\boldsymbol{B} \in \mathbb{R}^{n \times q}$ is the distribution matrix. $\boldsymbol{\eta} \in \mathbb{R}^n$ denotes the unknown disturbance and system uncertainty.

Taking the situation into account and the unknown fault, Eq (2.5) is extended to:

$$\begin{cases} \dot{\boldsymbol{x}} = \boldsymbol{G}(\boldsymbol{x}) + \boldsymbol{B}\boldsymbol{u} + \boldsymbol{D}\boldsymbol{f}_a + \boldsymbol{\eta} \\ \boldsymbol{y} = \boldsymbol{C}\boldsymbol{x} + \boldsymbol{d} \end{cases} \tag{2.6}$$

where $\boldsymbol{D} \in \mathbb{R}^{n\times q_f}$ is the fault distribution matrix and $\boldsymbol{f}_a \in \mathbb{R}^{q_f}$ is the unknown fault vector. $\boldsymbol{y} \in \mathbb{R}^n$ denotes the measured system output, and $\boldsymbol{C} \in \mathbb{R}^{n\times n}$ is the output distribution matrix. $\boldsymbol{d} \in \mathbb{R}^n$ denotes the measurement noise. In the real word, the fault $\boldsymbol{f}_a$, disturbance $\boldsymbol{\eta}$, and measurement noise $\boldsymbol{d}$ are bounded such as $\|\boldsymbol{f}_a\| \le \alpha_f < \infty$, $\|\boldsymbol{\eta}\| \le \overline{\eta} < \infty$, $\|\boldsymbol{d}\| \le \overline{d} < \infty$.

In this work, some assumptions are obtained as:

Assumption 1. *Matrices $\boldsymbol{C}$ and $\boldsymbol{D}$ satisfy that rank($\boldsymbol{C}\boldsymbol{D}$) = rank($\boldsymbol{D}$)*

3. Major results

3.1. Fault detection observer

In this section, a nonlinear observer is designed to achieve fault detection. When the HAA system (2.6) is under normal operation condition ($\boldsymbol{f}_a = 0$), the observer output approximates the system output and the residual is below a certain threshold. When a fault occurs, the observer would provide an accurate and timely alarm.

Let $\hat{\boldsymbol{x}} \in \mathbb{R}^n$ and $\hat{\boldsymbol{y}}$ denote the state estimation and observer output, respectively. For the nonlinear HAA system (2.6), construct the following fault detection observer

$$\begin{cases} \dot{\hat{\boldsymbol{x}}} = \boldsymbol{G}(\hat{\boldsymbol{x}}) + \boldsymbol{B}\boldsymbol{u} + \boldsymbol{L}(\hat{\boldsymbol{y}} - \boldsymbol{y}) \\ \hat{\boldsymbol{y}} = \boldsymbol{C}\hat{\boldsymbol{x}} \end{cases} \tag{3.1}$$

where $\boldsymbol{L}$ is the designed gain to make the observer (3.1) such that:

1) The error of state estimation $\boldsymbol{e}_x = \hat{\boldsymbol{x}} - \boldsymbol{x}$ should be convergent without system disturbance $\boldsymbol{\nu}$.

2) Under zero initial condition, when system disturbance $\boldsymbol{\nu}$ exists, and given an attenuation level $\sigma > 0$, the error of output $\boldsymbol{e}_y = \hat{\boldsymbol{y}} - \boldsymbol{y}$ satisfies $\mathcal{H}_\infty$ performance as

$$\|\boldsymbol{e}_y\|^2 \le \sigma\|\boldsymbol{\nu}\|^2 \tag{3.2}$$

To ensure these conditions, the LMI technique is used widespread to choose $\boldsymbol{L}$. In most studies, the inequation $2\boldsymbol{e}_x^T\boldsymbol{P}\Delta\boldsymbol{G} \le \alpha^2\boldsymbol{e}_x^T\boldsymbol{P}^2\boldsymbol{e}_x + \boldsymbol{e}_x^T\boldsymbol{e}_x$ is adopted to process the nonlinear estimation error part $\Delta\boldsymbol{G}$, where $\boldsymbol{P}^T = \boldsymbol{P} > 0$, $\Delta\boldsymbol{G} \triangleq \boldsymbol{G}(\hat{\boldsymbol{x}}) - \boldsymbol{G}(\boldsymbol{x})$. The solution of LMIs constrains the result of solving $\boldsymbol{L}$. To overcome the conservative constraint, for the nonlinear function, there is a lemma as following:

Lemma 3.1. *Under $\boldsymbol{\Pi}(\cdot) : \mathbb{R}^n \to \mathbb{R}^n$ is Lipschitz and given two vectors $\boldsymbol{x}, \boldsymbol{y} \in \mathbb{R}^n$, there is a function $\boldsymbol{\Xi} \triangleq \boldsymbol{\Xi}(\boldsymbol{x}, \boldsymbol{y}) : \mathbb{R}^n \times \mathbb{R}^n \to \mathbb{R}^{n\times n}$ such that $\boldsymbol{\Pi}(\boldsymbol{x}) - \boldsymbol{\Pi}(\boldsymbol{y}) = \boldsymbol{\Xi} \cdot (\boldsymbol{x} - \boldsymbol{y})$ and elements Ξ_{ij} bounded with $\underline{\Xi} \le \Xi_{ij} \le \overline{\Xi}$.*

Proof. Define a set of vectors $\boldsymbol{z}_i \in \mathbb{R}^n (i = 0, 1, 2..., n)$ as:

$$\boldsymbol{z}_i = \begin{cases} \boldsymbol{x}, & i = 0 \\ [y_1, ..., y_i, x_{i+1}, ..., x_n]^T, & i = 1, ..., n-1 \\ \boldsymbol{y}, & i = n \end{cases} \tag{3.3}$$

and functions $\boldsymbol{\xi}_j \triangleq \boldsymbol{\xi}_j(\boldsymbol{x}, \boldsymbol{y}) : \mathbb{R}^n \times \mathbb{R}^n \to \mathbb{R}^n, (j = 1, 2, ...n)$ as:

$$\boldsymbol{\xi}_j = \begin{cases} \mathbf{0}_n, & x_j = y_j \\ \dfrac{\boldsymbol{\Pi}(z_{j-1}) - \boldsymbol{\Pi}(z_j)}{x_j - y_j}, & x_j \neq y_j \end{cases} \tag{3.4}$$

Choose $\boldsymbol{\Xi} \triangleq \begin{bmatrix} \boldsymbol{\xi}_1 & \boldsymbol{\xi}_2 & \dots & \boldsymbol{\xi}_n \end{bmatrix}$, $\min(\boldsymbol{\xi}_j) \le \xi_{ij} \le \max(\boldsymbol{\xi}_j)$, then

$$\begin{aligned} \boldsymbol{\Xi} \cdot (\boldsymbol{x} - \boldsymbol{y}) &= \begin{bmatrix} \boldsymbol{\xi}_1 & \boldsymbol{\xi}_2 & \dots & \boldsymbol{\xi}_n \end{bmatrix} \begin{bmatrix} x_1 - y_1 \\ x_2 - y_2 \\ \vdots \\ x_n - y_n \end{bmatrix} \\ &= \boldsymbol{\Pi}(z_0) - \boldsymbol{\Pi}(z_1) + \boldsymbol{\Pi}(z_1) - \boldsymbol{\Pi}(z_2) + \cdots - \boldsymbol{\Pi}(z_n) \\ &= \boldsymbol{\Pi}(\boldsymbol{x}) - \boldsymbol{\Pi}(\boldsymbol{y}) \end{aligned} \tag{3.5}$$

The proof is completed. □

Let $\kappa = \sum_{j=1}^{n} \boldsymbol{\xi}_j \boldsymbol{e}_j^T$, where $\boldsymbol{e}_j \in \mathbb{R}^n$ is a vector whose jth component is 1 and others are 0. Then, matrix $\boldsymbol{\Xi}(\boldsymbol{\kappa})$ is parameterized and components of κ, which belong to a convex set $\mathcal{H}_n$ for which the set of vertices is defined $\mathcal{V} = \{\kappa \in \mathbb{R}^{n \times n} : \kappa_j \in \{\overline{\xi}_j, \underline{\xi}_j\}\}$. The state estimation error dynamics $\dot{\boldsymbol{e}}_x$ is given by

$$\dot{\boldsymbol{e}}_x = \dot{\hat{\boldsymbol{x}}} - \dot{\boldsymbol{x}} = \boldsymbol{G}(\hat{\boldsymbol{x}}) - \boldsymbol{G}(\boldsymbol{x}) + \boldsymbol{L}\boldsymbol{C}\boldsymbol{e}_x - \boldsymbol{\eta} - \boldsymbol{L}\boldsymbol{d} - \boldsymbol{D}\boldsymbol{f}_a \tag{3.6}$$

According to Lemma.3.1, dynamics (3.6) is reformulated to:

$$\dot{\boldsymbol{e}}_x = (\boldsymbol{\Xi}(\kappa) + \boldsymbol{L}\boldsymbol{C})\boldsymbol{e}_x + \boldsymbol{E}_d\boldsymbol{\nu} - \boldsymbol{D}\boldsymbol{f}_a \tag{3.7}$$

where disturbance $\boldsymbol{\nu} = \begin{bmatrix} \boldsymbol{d} \\ \boldsymbol{\eta} \end{bmatrix}$ and $\boldsymbol{E}_d = \begin{bmatrix} -\boldsymbol{L} & -\boldsymbol{I} \end{bmatrix}$.

Sufficient conditions for the stablity and $\mathtt{H}_\infty$ performance of system (3.6) is provided by the theorem:

Theorem 3.1. *Under fault free condition and* $\boldsymbol{L} = -\frac{1}{2}\boldsymbol{P}_D^{-1}\boldsymbol{C}^T$, *if there is a positive definite matrix* $\boldsymbol{P}_D \in \mathbb{R}^{n \times n}$ *and a prescibed attenuation level* $\sigma > 0$ *such that the inequality* $\boldsymbol{Q}_D < 0$, *then*

$$\boldsymbol{Q}_D = \begin{bmatrix} (\boldsymbol{\Xi}(\kappa) + \boldsymbol{L}\boldsymbol{C})^T \boldsymbol{P}_D + \boldsymbol{P}_D (\boldsymbol{\Xi}(\kappa) + \boldsymbol{L}\boldsymbol{C}) + \boldsymbol{C}^T\boldsymbol{C} & \boldsymbol{Q}_{D2} \\ * & \boldsymbol{E}_0^T\boldsymbol{E}_0 - \sigma^2\boldsymbol{I} \end{bmatrix} \tag{3.8}$$

where $\boldsymbol{Q}_{D2} = \boldsymbol{P}_D\boldsymbol{E}_d + \boldsymbol{C}^T\boldsymbol{E}_0$, $\boldsymbol{E}_0 = \begin{bmatrix} -\boldsymbol{I} & \mathbf{0} \end{bmatrix}$. $\mathbf{0}$ *denotes a matrix whose components are 0 with appropriate dimension.*

Then, the state estimation error dynamic (3.6) *asymptotically converges to zero with* $\boldsymbol{\nu} = 0$ *and satisfies* $\mathtt{H}_\infty$ *performance with* $\boldsymbol{\nu} \neq 0$.

Proof. 1) Choose the electable Lyapunov function as $\boldsymbol{V} = \boldsymbol{e}_x^T\boldsymbol{P}_D\boldsymbol{e}_x > 0$, then

$$\begin{aligned} \dot{\boldsymbol{V}} &= \boldsymbol{e}_x^T[(\boldsymbol{\Xi}(\kappa) + \boldsymbol{L}\boldsymbol{C})^T\boldsymbol{P}_D + \boldsymbol{P}_D(\boldsymbol{\Xi}(\kappa) + \boldsymbol{L}\boldsymbol{C})]\boldsymbol{e}_x + \boldsymbol{\nu}^T\boldsymbol{E}_d^T\boldsymbol{P}_D\boldsymbol{e}_x + \boldsymbol{e}_x^T\boldsymbol{P}_D\boldsymbol{E}_d\boldsymbol{\nu} \\ &= \begin{bmatrix} \boldsymbol{e}_x \\ \boldsymbol{\nu} \end{bmatrix}^T \begin{bmatrix} (\boldsymbol{\Xi}(\kappa) + \boldsymbol{L}\boldsymbol{C})^T\boldsymbol{P}_D + \boldsymbol{P}_D(\boldsymbol{\Xi}(\kappa) + \boldsymbol{L}\boldsymbol{C}) & \boldsymbol{P}_D\boldsymbol{E}_d \\ \boldsymbol{E}_d^T\boldsymbol{P}_D & \mathbf{0} \end{bmatrix} \begin{bmatrix} \boldsymbol{e}_x \\ \boldsymbol{\nu} \end{bmatrix} \end{aligned}$$

If $\boldsymbol{Q}_D \leq 0$ holds, then the inequality $\boldsymbol{Q}_{D1}$ satisfies that

$$\boldsymbol{Q}_{D1} = \begin{bmatrix} (\boldsymbol{\Xi}(\kappa) + \boldsymbol{LC})^T \boldsymbol{P}_D + \boldsymbol{P}_D(\boldsymbol{\Xi}(\kappa) + \boldsymbol{LC}) & \boldsymbol{Q}_{D2} \\ * & -\sigma^2 \boldsymbol{I} \end{bmatrix} < 0$$

According to the Schur Inequality lemma, $\boldsymbol{Q}_{D1} < 0$ is equal to $(\boldsymbol{\Xi}(\kappa) + \boldsymbol{LC})^T \boldsymbol{P}_D + \boldsymbol{P}_D (\boldsymbol{\Xi}(\kappa) + \boldsymbol{LC}) \leq 0$. Hence, when $\boldsymbol{\nu} = 0$ holds, $\dot{\boldsymbol{V}} < 0$ is obtained, which means that the state estimation error dynamic (3.6) is stable asymptotically.

2) Subsequently, consider the disturbance $\boldsymbol{\nu} \neq 0$. The norm of output error $\boldsymbol{e}_y = \boldsymbol{Ce}_x - \boldsymbol{d}$ is given by:

$$\|\boldsymbol{e}_y\|^2 = \boldsymbol{e}_y^T \boldsymbol{e}_y = \begin{bmatrix} \boldsymbol{e}_x \\ \boldsymbol{\nu} \end{bmatrix}^T \begin{bmatrix} \boldsymbol{C}^T \boldsymbol{C} & \boldsymbol{C}^T \boldsymbol{E}_0 \\ * & \boldsymbol{E}_0^T \boldsymbol{E}_0 \end{bmatrix} \begin{bmatrix} \boldsymbol{e}_x \\ \boldsymbol{\nu} \end{bmatrix}$$

Define a performance index $\boldsymbol{J}_d = \dot{\boldsymbol{V}} + \boldsymbol{e}_y^T \boldsymbol{e}_y - \sigma^2 \boldsymbol{\nu}^T \boldsymbol{\nu}$, and rewrite $\boldsymbol{J}_d$ as a matrix form

$$\boldsymbol{J}_d = \begin{bmatrix} \boldsymbol{e}_x \\ \boldsymbol{\nu} \end{bmatrix}^T \begin{bmatrix} (\boldsymbol{\Xi}(\kappa) + \boldsymbol{LC})^T \boldsymbol{P}_D + \boldsymbol{P}_D (\boldsymbol{\Xi}(\kappa) + \boldsymbol{LC}) + \boldsymbol{C}^T \boldsymbol{C} & \boldsymbol{Q}_{D2} \\ * & \boldsymbol{E}_0^T \boldsymbol{E}_0 - \sigma^2 \boldsymbol{I} \end{bmatrix} \begin{bmatrix} \boldsymbol{e}_x \\ \boldsymbol{\nu} \end{bmatrix} \tag{3.9}$$

$\boldsymbol{J}_d < 0$ is obtained if $\boldsymbol{Q}_D < 0$ is satisfied. Under the zero initial condition, the integral of $\boldsymbol{J}_d$ is obtained as:

$$\begin{aligned} &\int_0^T \boldsymbol{J}_d \, dt = \boldsymbol{V}(T) - \boldsymbol{V}(0) + \int_0^T \left(\boldsymbol{e}_y^T \boldsymbol{e}_y - \sigma^2 \boldsymbol{\nu}^T \boldsymbol{\nu} \right) dt < 0 \\ &\rightarrow \int_0^T \left(\boldsymbol{e}_y^T \boldsymbol{e}_y - \sigma^2 \boldsymbol{\nu}^T \boldsymbol{\nu} \right) dt < 0 \end{aligned} \tag{3.10}$$

which means the performance with Eq (3.2) is obtained.
The proof is complete. □

The occurrence of fault means that the system is under an abnormal state, which is extracted from the output error $\boldsymbol{e}_y$ with an appropriate residual evaluation function. The dimension of states is different, and the output error is required to be normalized. In the non-failure system operation state, $\|\boldsymbol{e}_y\|^2 \leq \sigma \|\boldsymbol{\nu}\|^2$ is satisfying. Hence, there exist $\underline{\boldsymbol{e}} = \inf(\boldsymbol{e}_y) = \begin{bmatrix} \underline{e}_1 \\ \vdots \\ \underline{e}_n \end{bmatrix}$ and $\overline{\boldsymbol{e}} = \sup(\boldsymbol{e}_y) = \begin{bmatrix} \overline{e}_1 \\ \vdots \\ \overline{e}_n \end{bmatrix}$. Choose a new state $\boldsymbol{e} = \begin{bmatrix} e_1 \\ \vdots \\ e_n \end{bmatrix} = \begin{bmatrix} (e_{y,1} - \underline{e}_1)/(\overline{e}_1 - \underline{e}_1) \\ \vdots \\ (e_{y,n} - \underline{e}_n)/(\overline{e}_n - \underline{e}_n) \end{bmatrix}$, where $e_{y,i}$ is the ith element of $\boldsymbol{e}_y$. Subsequently, choose the residual evaluation function $\|\boldsymbol{\chi}_D\|^2 = \left(\int_{t_1}^{t_2} \boldsymbol{\chi}_D^T \boldsymbol{\chi}_D \, dt \right)^{1/2}$ with a finite time window $t \in (t_1, t_2]$, where

$$\boldsymbol{\chi}_D = \begin{bmatrix} \max\left(\max(e_1 - 1, 0), \max(0 - e_1, 0)\right) \\ \vdots \\ \max\left(\max(e_n - 1, 0), \max(0 - e_n, 0)\right) \end{bmatrix} \tag{3.11}$$

In non-fault condition, the evaluation function $\|\boldsymbol{\chi}_D\|^2 = 0$. If $\|\boldsymbol{\chi}_D\|^2 > 0$ holds, and it means that there is an unknown fault occurring.

3.2. Fault isolation observer

When there is fault occurring, $\|\chi_D\|^2 > 0$ holds and gives the fault alarm. However, other information about the fault $\boldsymbol{f}_a$ cannot be provided. Identifying the faulty component accurately contributes to executing the failure policy accordingly, which is the target of the fault isolation observer.

Without loss of generality, it is assumed that there is only one faulty component. The system state equation (2.6) is extended for each actuator component as:

$$\dot{\boldsymbol{x}}^i = \boldsymbol{G}^i + \boldsymbol{B}\boldsymbol{u} + \boldsymbol{\eta} + \boldsymbol{D}^i \boldsymbol{f}_a^i \tag{3.12}$$

where $\boldsymbol{G}^i \triangleq \boldsymbol{G}(\boldsymbol{x}^i)$. $\boldsymbol{f}_a^i$ denotes the fault from the ith actuator component and $\boldsymbol{D}^i \in \mathbb{R}^n, (i = 1, 2, ..., q)$ denotes the ith column of the matrix $\boldsymbol{B}$ to match the corresponding distribution. Moreover, a bank of nonlinear observers can be constructed for the ith actuator component as:

$$\begin{cases} \dot{\boldsymbol{\delta}}^i = \boldsymbol{N}^i \boldsymbol{\delta}^i + \boldsymbol{M}^i \boldsymbol{u} + \boldsymbol{T}^i \hat{\boldsymbol{G}}^i + \boldsymbol{H}^i \boldsymbol{y} \\ \hat{\boldsymbol{x}}^i = \boldsymbol{\delta}^i + \boldsymbol{R}^i \boldsymbol{y} \\ \hat{\boldsymbol{y}}^i = \boldsymbol{C}\hat{\boldsymbol{x}}^i \end{cases} \tag{3.13}$$

where $\hat{\boldsymbol{G}}^i \triangleq \boldsymbol{G}(\hat{\boldsymbol{x}}^i)$. $\hat{\boldsymbol{x}}^i$, $\hat{\boldsymbol{y}}^i$ are the estimation of $\boldsymbol{x}^i$ and $\boldsymbol{y}$, respectively. $\boldsymbol{M}^i, \boldsymbol{T}^i, \boldsymbol{H}^i, \boldsymbol{N}^i$, and $\boldsymbol{R}^i$ are matrices to be solved. The esitmation error dynamics $\dot{\boldsymbol{e}}_x^i = \dot{\hat{\boldsymbol{x}}}^i - \dot{\boldsymbol{x}}^i$ is as follows:

$$\begin{aligned} \dot{\boldsymbol{e}}_x^i &= \boldsymbol{N}^i \boldsymbol{\delta}^i + \boldsymbol{M}^i \boldsymbol{u} + \boldsymbol{T}\hat{\boldsymbol{G}}^i + \boldsymbol{H}^i \boldsymbol{y} + \boldsymbol{R}^i \boldsymbol{C}\dot{\boldsymbol{x}}^i + \boldsymbol{R}^i \dot{\boldsymbol{d}} - \dot{\boldsymbol{x}}^i \\ &= \boldsymbol{N}^i \hat{\boldsymbol{x}}^i + \boldsymbol{M}^i \boldsymbol{u} + \boldsymbol{T}^i \hat{\boldsymbol{G}}^i + \left(\boldsymbol{H}^i - \boldsymbol{N}^i \boldsymbol{R}^i\right) \boldsymbol{y} + \left(\boldsymbol{R}^i \boldsymbol{C} - \boldsymbol{I}\right) \dot{\boldsymbol{x}}^i + \boldsymbol{R}^i \dot{\boldsymbol{d}} \\ &= \boldsymbol{N}^i \boldsymbol{e}_x^i + \left(\boldsymbol{N}^i + \boldsymbol{H}^i \boldsymbol{C} - \boldsymbol{N}^i \boldsymbol{R}^i \boldsymbol{C}\right) \boldsymbol{x}^i + \left(\boldsymbol{M}^i + \boldsymbol{R}^i \boldsymbol{C}\boldsymbol{B} - \boldsymbol{B}\right) \boldsymbol{u} + \boldsymbol{T}^i \hat{\boldsymbol{G}} + \left(\boldsymbol{R}^i \boldsymbol{C} - \boldsymbol{I}\right) \boldsymbol{G} \\ &\quad + \left(\boldsymbol{R}^i \boldsymbol{C} - \boldsymbol{I}\right) \boldsymbol{\eta} + \left(\boldsymbol{H}^i - \boldsymbol{N}^i \boldsymbol{R}^i\right) \boldsymbol{d} + \boldsymbol{R}^i \dot{\boldsymbol{d}} + \left(\boldsymbol{R}^i \boldsymbol{C} - \boldsymbol{I}\right) \boldsymbol{D}^i \boldsymbol{f}_a^i \\ \boldsymbol{e}_y^i &= \boldsymbol{C}\boldsymbol{e}_x^i - \boldsymbol{d} \end{aligned} \tag{3.14}$$

Choose matrices following conditions:

$$\boldsymbol{N}^i + \boldsymbol{H}^i \boldsymbol{C} - \boldsymbol{N}^i \boldsymbol{R}^i \boldsymbol{C} = 0, \tag{3.15a}$$

$$\boldsymbol{T}^i = \boldsymbol{I} - \boldsymbol{R}^i \boldsymbol{C}, \tag{3.15b}$$

$$\boldsymbol{M}^i = \boldsymbol{T}^i \boldsymbol{B}, \tag{3.15c}$$

such that the estimation error dynamic (3.14) is simplified to

$$\dot{\boldsymbol{e}}_x^i = \boldsymbol{N}^i \boldsymbol{e}_x^i + \boldsymbol{T}^i \left(\hat{\boldsymbol{G}} - \boldsymbol{G}\right) - \boldsymbol{T}^i \boldsymbol{\eta} + \left(\boldsymbol{H}^i - \boldsymbol{N}^i \boldsymbol{R}^i\right) \boldsymbol{d} + \boldsymbol{R}^i \dot{\boldsymbol{d}} - \boldsymbol{T}^i \boldsymbol{D}^i \boldsymbol{f}_a^i, \tag{3.16a}$$

$$\boldsymbol{e}_y^i = \boldsymbol{C}\boldsymbol{e}_x^i - \boldsymbol{d} \tag{3.16b}$$

The estimation error dynamics $\dot{\boldsymbol{e}}_x^i$ is sensitive to other component faults $\boldsymbol{f}_a^j (j \neq i)$ when the effect caused by $\boldsymbol{f}_a^i$ can be decoupled. To ensure this, $\boldsymbol{T}^i \boldsymbol{D}^i = \boldsymbol{0}$ and $\boldsymbol{T}^i \boldsymbol{B}^j \neq \boldsymbol{0}$ should be held simultaneously, where $\boldsymbol{B}^j$ denotes any column of $\boldsymbol{B}$ but the ith one. One solution can be chosen as $\boldsymbol{R}^i = \boldsymbol{D}^i (\boldsymbol{C}\boldsymbol{D}^i)^+$, where $(\cdot)^+$ denotes the generalized inverse of $(\cdot)$. The matrices $\boldsymbol{T}^i$ and $\boldsymbol{M}^i$ would be obtained with (3.15b) and (3.15c).

Choosing a parameter matrix $\boldsymbol{K}^i$ such that $\boldsymbol{N}^i = \boldsymbol{K}^i\boldsymbol{C}$. Then, $\boldsymbol{H}^i = \boldsymbol{K}^i\boldsymbol{C}\boldsymbol{R}^i - \boldsymbol{K}^i$ is obtained based on condition (3.15a). Under Lemma 3.1, the estimation error dynamic is reformed to:

$$\dot{\boldsymbol{e}}_x^i = \left(\boldsymbol{N}^i + \boldsymbol{T}^i\boldsymbol{\Xi}^i(\kappa)\right)\boldsymbol{e}_x^i + \boldsymbol{E}_i\boldsymbol{\nu} \tag{3.17}$$

where $\boldsymbol{E}_i = \begin{bmatrix} -\boldsymbol{K}^i & \boldsymbol{T}^i & \boldsymbol{R}^i \end{bmatrix}$, $\boldsymbol{\nu} = \begin{bmatrix} \boldsymbol{d} \\ \boldsymbol{\eta} \\ \dot{\boldsymbol{d}} \end{bmatrix}$. Then, the output error $\boldsymbol{e}_y^i = \boldsymbol{C}\boldsymbol{e}_x^i + \boldsymbol{E}_0^i\boldsymbol{\nu}$, where $\boldsymbol{E}_0^i = \begin{bmatrix} -\boldsymbol{I} & \boldsymbol{0} & \boldsymbol{0} \end{bmatrix}$.

Sufficient conditions for the stablity and $\mathtt{H}_\infty$ performance of system with $\boldsymbol{\nu}$ (3.16) is provided by the theorem:

Theorem 3.2. *Under the fautl-free condition and $\boldsymbol{K}^i = -\frac{1}{2}(\boldsymbol{P}_I^i)^{-1}\boldsymbol{C}^T$, if there exists a positive definite matrix $\boldsymbol{P}_I^i \in \mathbb{R}^{n\times n}$ and a prescibed attenuation level $\sigma_i > 0$ such that the inequality $\boldsymbol{Q}_I \le 0$, then*

$$\boldsymbol{Q}_I = \begin{bmatrix} (\boldsymbol{N}^i + \boldsymbol{T}^i\boldsymbol{\Xi}^i(\kappa))^T\boldsymbol{P}_I^i + \boldsymbol{P}_I^i(\boldsymbol{N}^i + \boldsymbol{T}^i\boldsymbol{\Xi}^i(\kappa)) + \boldsymbol{C}^T\boldsymbol{C} & \boldsymbol{Q}_{I2} \\ * & (\boldsymbol{E}_0^i)^T\boldsymbol{E}_0^i - \sigma_i^2\boldsymbol{I} \end{bmatrix} \tag{3.18}$$

$\boldsymbol{Q}_{I2} = \boldsymbol{P}_I^i\boldsymbol{E}_i + \boldsymbol{C}^T\boldsymbol{E}_0^i$. *Then, the state estimation error dynamic* (3.14) *asymptotically converges to zero with $\boldsymbol{\nu} = 0$ and satisfies $\mathtt{H}_\infty$ performance with $\boldsymbol{\nu} \neq 0$.*

Proof. The proof of Theorem.3.2 is similar to that of Theorem.3.1 by using the state error dynamics $\dot{\boldsymbol{e}}_x^i$.

Define indicator functions $\boldsymbol{\chi}_I^i$ for each observer in (3.13). When the ith actuator component malfunctions, the effect on the matched ith observer would be offset by $T^iD^i = \boldsymbol{0}$. Hence, the ith faulty component is isolated when the evaluation function $\|\boldsymbol{\chi}_I^i\|^2 = 0$ holds but others $\|\boldsymbol{\chi}_I^j\|^2 > 1 (j \neq i)$ concurrently.

3.3. Fault reconstruction observer

The observer (3.1) monitors the occurrence of failures, which means determining if unknown $\boldsymbol{D}\boldsymbol{f}_a$ exists. The bank of observers (3.13) identifies the faulty component, which means matrix $\boldsymbol{D}$ is provided. In the fault countermeasure, the size of fault links with the fault compensate scheme. In this section, a nonlinear robust fault reconstruct observer is devoted to estimate the unknown fault and state simultaneously. Consider a new state vector $\overline{\boldsymbol{x}} = \begin{bmatrix} \boldsymbol{x} \\ \boldsymbol{f}_a \end{bmatrix} \in \mathbb{R}^{(n+q_f)}$, then system (2.6) is extended to the descriptor nonlinear system as:

$$\begin{cases} \underbrace{\begin{bmatrix} \boldsymbol{I} & \boldsymbol{0} \\ \boldsymbol{0} & \boldsymbol{0} \end{bmatrix}}_{\overline{\boldsymbol{E}}}\dot{\overline{\boldsymbol{x}}} = \underbrace{\begin{bmatrix} \boldsymbol{0} & \boldsymbol{D} \\ \boldsymbol{0} & \boldsymbol{I} \end{bmatrix}}_{\overline{\boldsymbol{A}}}\overline{\boldsymbol{x}} + \underbrace{\begin{bmatrix} \boldsymbol{I} \\ \boldsymbol{0} \end{bmatrix}}_{\overline{\boldsymbol{D}}_G}\boldsymbol{G}(\boldsymbol{x}) + \underbrace{\begin{bmatrix} \boldsymbol{B} \\ \boldsymbol{0} \end{bmatrix}}_{\overline{\boldsymbol{B}}}\boldsymbol{u} + \underbrace{\begin{bmatrix} \boldsymbol{0} \\ -\boldsymbol{I} \end{bmatrix}}_{\overline{\boldsymbol{D}}_f}\boldsymbol{f}_a + \underbrace{\begin{bmatrix} \boldsymbol{I} & \boldsymbol{0} \\ \boldsymbol{0} & \boldsymbol{0} \end{bmatrix}}_{\overline{\boldsymbol{D}}_{v1}}\underbrace{\begin{bmatrix} \boldsymbol{\eta} \\ \boldsymbol{d} \end{bmatrix}}_{\overline{\boldsymbol{\nu}}} \\ \boldsymbol{y} = \underbrace{\begin{bmatrix} \boldsymbol{C} & \boldsymbol{0} \end{bmatrix}}_{\overline{\boldsymbol{C}}}\overline{\boldsymbol{x}} + \underbrace{\begin{bmatrix} \boldsymbol{0} & \boldsymbol{I} \end{bmatrix}}_{\overline{\boldsymbol{D}}_{v2}}\begin{bmatrix} \boldsymbol{\eta} \\ \boldsymbol{d} \end{bmatrix} \end{cases} \tag{3.19}$$

Choose a matrix $\boldsymbol{V} \in \mathbb{R}^{q_f \times (n+q_f)}$, which satifies that

$$\boldsymbol{V}\overline{\boldsymbol{E}} = \boldsymbol{0} \tag{3.20}$$

Then, define matrices $\tilde{\boldsymbol{H}}$ and $\tilde{\boldsymbol{C}}$ such as:

$$\tilde{\boldsymbol{H}} = \begin{bmatrix} \boldsymbol{V}\overline{\boldsymbol{D}}_G & \boldsymbol{V}\overline{\boldsymbol{D}}_f \\ \boldsymbol{0} & \boldsymbol{0} \end{bmatrix} \tag{3.21a}$$

$$\tilde{\boldsymbol{C}} = \left(\boldsymbol{I} - \tilde{\boldsymbol{H}}\tilde{\boldsymbol{H}}^{+}\right)\begin{bmatrix} \tilde{\boldsymbol{H}}\tilde{\boldsymbol{A}} \\ \boldsymbol{C} \end{bmatrix} \tag{3.21b}$$

Consider the following observer for system (3.19)

$$\begin{cases} \dot{\boldsymbol{\zeta}} = \boldsymbol{N}\boldsymbol{\zeta} + \boldsymbol{J}\boldsymbol{u} + \boldsymbol{T}\overline{\boldsymbol{D}}_G\hat{\boldsymbol{G}} + \boldsymbol{H}\left(\boldsymbol{I} - \tilde{\boldsymbol{H}}\tilde{\boldsymbol{H}}^{+}\right)\begin{bmatrix} -\boldsymbol{V}\overline{\boldsymbol{B}}\boldsymbol{u} \\ \boldsymbol{y} \end{bmatrix} \\ \hat{\overline{\boldsymbol{x}}} = \boldsymbol{Q}\boldsymbol{\zeta} + \boldsymbol{R}\left(\boldsymbol{I} - \tilde{\boldsymbol{H}}\tilde{\boldsymbol{H}}^{+}\right)\begin{bmatrix} -\boldsymbol{V}\boldsymbol{B}\boldsymbol{u} \\ \boldsymbol{y} \end{bmatrix} \end{cases} \tag{3.22}$$

where

$$\begin{aligned} \left(\boldsymbol{I} - \tilde{\boldsymbol{H}}\tilde{\boldsymbol{H}}^{+}\right)\begin{bmatrix} -\boldsymbol{V}\overline{\boldsymbol{B}}\boldsymbol{u} \\ \boldsymbol{y} \end{bmatrix} &= \left(\boldsymbol{I} - \tilde{\boldsymbol{H}}\tilde{\boldsymbol{H}}^{+}\right)\left(\begin{bmatrix} \boldsymbol{V}\overline{\boldsymbol{A}}\overline{\boldsymbol{x}} \\ \overline{\boldsymbol{C}}\overline{\boldsymbol{x}} \end{bmatrix} + \begin{bmatrix} \boldsymbol{V}\overline{\boldsymbol{D}}_G & \boldsymbol{V}\overline{\boldsymbol{D}}_f \\ \boldsymbol{0} & \boldsymbol{0} \end{bmatrix}\begin{bmatrix} \boldsymbol{G}(\boldsymbol{x}) \\ \boldsymbol{f}_a \end{bmatrix} + \begin{bmatrix} \boldsymbol{V}\overline{\boldsymbol{D}}_{v1} \\ \boldsymbol{V}\overline{\boldsymbol{D}}_{v2} \end{bmatrix}\overline{\boldsymbol{v}}\right) \\ &= \tilde{\boldsymbol{C}}\overline{\boldsymbol{x}} + \underbrace{\left(\boldsymbol{I} - \tilde{\boldsymbol{H}}\tilde{\boldsymbol{H}}^{+}\right)\begin{bmatrix} \boldsymbol{V}\overline{\boldsymbol{D}}_{v1} \\ \boldsymbol{V}\overline{\boldsymbol{D}}_{v2} \end{bmatrix}}_{\tilde{\boldsymbol{D}}_v}\overline{\boldsymbol{v}} \\ &= \tilde{\boldsymbol{C}}\overline{\boldsymbol{x}} + \tilde{\boldsymbol{D}}_v\overline{\boldsymbol{v}} \end{aligned} \tag{3.23}$$

Define the error $\boldsymbol{\varsigma} = \boldsymbol{\zeta} - \boldsymbol{T}\overline{\boldsymbol{E}}\overline{\boldsymbol{x}}$, an error dynamic is obtained as:

$$\begin{cases} \dot{\boldsymbol{\varsigma}} = \dot{\boldsymbol{\zeta}} - \boldsymbol{T}\overline{\boldsymbol{E}}\dot{\overline{\boldsymbol{x}}} = \boldsymbol{N}\left(\boldsymbol{\zeta} - \boldsymbol{T}\overline{\boldsymbol{E}}\overline{\boldsymbol{x}}\right) + (\boldsymbol{J} - \boldsymbol{T}\boldsymbol{B})\,\boldsymbol{u} + \boldsymbol{T}\Delta\overline{\boldsymbol{G}} + \left(\boldsymbol{N}\boldsymbol{T}\overline{\boldsymbol{E}} + \tilde{\boldsymbol{C}} - \boldsymbol{T}\overline{\boldsymbol{A}}\right)\overline{\boldsymbol{x}} \\ \qquad\qquad + \underbrace{\left(\tilde{\boldsymbol{D}}_v - \boldsymbol{T}\overline{\boldsymbol{D}}_{v1}\right)}_{\tilde{\boldsymbol{D}}_{v1}}\overline{\boldsymbol{v}} \\ \boldsymbol{e} = \begin{bmatrix} \boldsymbol{e}_x \\ \boldsymbol{e}_f \end{bmatrix} = \hat{\overline{\boldsymbol{x}}} - \overline{\boldsymbol{x}} = \boldsymbol{Q}\left(\boldsymbol{\zeta} - \boldsymbol{T}\overline{\boldsymbol{E}}\overline{\boldsymbol{x}}\right) + \left(\boldsymbol{R}\tilde{\boldsymbol{C}} + \boldsymbol{Q}\boldsymbol{T}\overline{\boldsymbol{E}} - \boldsymbol{I}\right)\overline{\boldsymbol{x}} + \underbrace{\boldsymbol{R}\tilde{\boldsymbol{D}}_v}_{\tilde{\boldsymbol{D}}_{v2}}\overline{\boldsymbol{v}} \end{cases} \tag{3.24}$$

where $\Delta\overline{\boldsymbol{G}} = \overline{\boldsymbol{D}}_G\left(\hat{\boldsymbol{G}} - \boldsymbol{G}\right)$. If there are matrices $\boldsymbol{T}, \boldsymbol{N}, \boldsymbol{J}, \boldsymbol{H}, \boldsymbol{Q}$, and $\boldsymbol{R}$ satisfy that:

$$\boldsymbol{N}\boldsymbol{T}\overline{\boldsymbol{E}} + \tilde{\boldsymbol{C}} - \boldsymbol{T}\overline{\boldsymbol{A}} = \boldsymbol{0}, \tag{3.25a}$$

$$\boldsymbol{R}\tilde{\boldsymbol{C}} + \boldsymbol{Q}\boldsymbol{T}\overline{\boldsymbol{E}} - \boldsymbol{I} = \boldsymbol{0}, \tag{3.25b}$$

$$\boldsymbol{J} - \boldsymbol{T}\boldsymbol{B} = \boldsymbol{0}, \tag{3.25c}$$

the error system(3.24) is converted to:

$$\begin{cases} \dot{\boldsymbol{\varsigma}} = \boldsymbol{N}\boldsymbol{\varsigma} + \boldsymbol{T}\Delta\overline{\boldsymbol{G}} + \tilde{\boldsymbol{D}}_{v1}\overline{\boldsymbol{v}} \\ \boldsymbol{e} = \boldsymbol{Q}\boldsymbol{\varsigma} + \tilde{\boldsymbol{D}}_{v2}\overline{\boldsymbol{v}} \end{cases} \tag{3.26}$$

Under Lemma.3.1, $\Delta\overline{\boldsymbol{G}} = \begin{bmatrix} \boldsymbol{\Xi}(\kappa) & \boldsymbol{0} \\ \boldsymbol{0} & \boldsymbol{0} \end{bmatrix} \boldsymbol{e} = \overline{\boldsymbol{\Xi}}(\kappa)\boldsymbol{e}$ is obtained.

In error system (3.26), the asymptotic stability of $\boldsymbol{\varsigma}$ ensures that $\lim_{t\to\infty} \boldsymbol{e} = 0$ for $\overline{\boldsymbol{\nu}} = 0$ sufficiently. When $\overline{\boldsymbol{\nu}} \neq 0$, matrices $\boldsymbol{T}, \boldsymbol{N}, \boldsymbol{J}, \boldsymbol{H}, \boldsymbol{Q}$, and $\boldsymbol{R}$ are designed to satisfy the $\mathtt{H}_\infty$ performance $\|\boldsymbol{e}\|^2 \leq \sigma_e \|\overline{\boldsymbol{\nu}}\|^2$ and condition (3.25) simultaneously. The sufficient condition is provided by the following theorem:

Theorem 3.3. *If there exists a positive definite matrix $\boldsymbol{P}_e \in \mathbb{R}^{(n+q_f)\times(n+q_f)}$ and a prescibed attenuation level $\sigma_e > 0$ such that the inequality $\boldsymbol{Q}_E \leq 0$, then*

$$\boldsymbol{Q}_E = \begin{bmatrix} \boldsymbol{N}^T\boldsymbol{P}_e + \boldsymbol{P}_e^T\boldsymbol{N} + \boldsymbol{P}_e\boldsymbol{P}_e & \boldsymbol{P}_e\boldsymbol{T}\overline{\boldsymbol{\Xi}}(\kappa) + \left(\boldsymbol{T}\overline{\boldsymbol{\Xi}}(\kappa)\right)^T\boldsymbol{P}_e & \boldsymbol{P}_e\left(\tilde{\boldsymbol{D}}_{v1} + \tilde{\boldsymbol{D}}_{v2}\right) + \left(\tilde{\boldsymbol{D}}_{v1} + \tilde{\boldsymbol{D}}_{v2}\right)^T\boldsymbol{P}_e \\ * & 0 & 0 \\ * & * & \tilde{\boldsymbol{D}}_{v2}^T\tilde{\boldsymbol{D}}_{v2} - \sigma_e^2\boldsymbol{I} \end{bmatrix} \tag{3.27}$$

Then, the error system (3.26) *asymptotically converges to zero with $\overline{\boldsymbol{\nu}} = 0$ and has $\mathtt{H}_\infty$ performance with $\overline{\boldsymbol{\nu}} \neq 0$.*

Proof. 1) Under $\overline{\boldsymbol{\nu}} = 0$, choose the electable Lyapunov function $\boldsymbol{V} = \boldsymbol{\varsigma}^T\boldsymbol{P}_e\boldsymbol{\varsigma}$, then

$$\begin{aligned} \dot{\boldsymbol{V}} &= \dot{\boldsymbol{\varsigma}}\boldsymbol{P}_e\boldsymbol{\varsigma} + \boldsymbol{\varsigma}^T\boldsymbol{P}_e\dot{\boldsymbol{\varsigma}} \\ &= \begin{bmatrix} \boldsymbol{\varsigma} \\ \boldsymbol{e} \end{bmatrix}^T \begin{bmatrix} \boldsymbol{N}^T\boldsymbol{P}_e + \boldsymbol{P}_e^T\boldsymbol{N} & \boldsymbol{P}_e\boldsymbol{T}\overline{\boldsymbol{\Xi}}(\kappa) + \left(\boldsymbol{T}\overline{\boldsymbol{\Xi}}(\kappa)\right)^T\boldsymbol{P}_e \\ * & 0 \end{bmatrix} \begin{bmatrix} \boldsymbol{\varsigma} \\ \boldsymbol{e} \end{bmatrix} \end{aligned} \tag{3.28}$$

When $\boldsymbol{Q}_E \leq 0$ holds, $\left(\boldsymbol{Q}_E - \begin{bmatrix} \boldsymbol{P}_e^T\boldsymbol{P}_e & 0 & 0 \\ 0 & 0 & 0 \\ 0 & 0 & \tilde{\boldsymbol{D}}_{v2}^T\tilde{\boldsymbol{D}}_{v2} \end{bmatrix}\right) \leq 0$ is given, which leads to $\dot{\boldsymbol{V}} \leq 0$. Hence, the error system (3.26) has asymptotic stability for $\overline{\boldsymbol{\nu}} = 0$.

2) When $\overline{\boldsymbol{\nu}} \neq 0$, the inequality

$$\boldsymbol{J}_e = \dot{\boldsymbol{V}} + \boldsymbol{e}^T\boldsymbol{e} - \sigma_e\overline{\boldsymbol{\nu}}^T\overline{\boldsymbol{\nu}} = \begin{bmatrix} \boldsymbol{\varsigma} \\ \boldsymbol{e} \\ \overline{\boldsymbol{\nu}} \end{bmatrix}^T \boldsymbol{Q}_E \begin{bmatrix} \boldsymbol{\varsigma} \\ \boldsymbol{e} \\ \overline{\boldsymbol{\nu}} \end{bmatrix} \leq 0$$

if $\boldsymbol{Q}_E \leq 0$ holds. Hence, the integral $\int_0^T \boldsymbol{J}_e\, dt = \boldsymbol{V} + \int_0^T \left(\boldsymbol{e}_y^T\boldsymbol{e}_y - \sigma^2\boldsymbol{\nu}^T\boldsymbol{\nu}\right) dt \leq 0$

This completes the proof. □

The fault estimation $\hat{\boldsymbol{f}}_a$ will be got from the state estimation $\hat{\overline{\boldsymbol{x}}} = \begin{bmatrix} \hat{\boldsymbol{x}} \\ \hat{\boldsymbol{f}}_a \end{bmatrix}$.

4. Application to the HAA

In this section, an HAA simulation system is used to illustrate the applicability and effectiveness of the proposed FD method.

Considering the engineering practice, there are $q = 5$ propulsion propellers employed to constitute actuators. With the HAA structure shown in Figure 1, Propeller 1 to 4 produce forward propulsive thrust mainnly, and pitch and yaw moments are produced by differential thrust from propellers.

Propeller 5 is is reversible, and thrust direction is crosswise with axis $O_b x$ to provide a yawing moment. The system input $\boldsymbol{u} = \begin{bmatrix} r_1 \\ \vdots \\ r_q \end{bmatrix}$ denotes the rotational speed of each propeller, which can be measured by revolution speed transducer due to the thrust $\boldsymbol{F}_P = \mathbf{R}_p \boldsymbol{u}$ is immeasurable, where $\mathbf{R}_p \in \mathbb{R}^{q\times q}$ is the conversion matrix of the rotate speed to force. The distribution matrix $\boldsymbol{B} = (\boldsymbol{I} - diag(\boldsymbol{\rho}))\begin{bmatrix} \mathbf{0} \\ \mathbf{M}^{-1}\mathbf{D}_p\mathbf{R}_p \end{bmatrix} \in \mathbb{R}^{n\times q}$, where $diag(\boldsymbol{\rho})$ is the actuator efficiency loss constant matrix (without fault, $\rho_i = 1$) and $\mathbf{D}_p$ is the arrangement matrix of propellers, which is designed as following:

$$\mathbf{D}_p = \begin{bmatrix} 1 & 1 & 1 & 1 & 0 \\ 0 & 0 & 0 & 0 & 1 \\ 0 & 0 & 0 & 0 & 0 \\ 0 & 0 & 0 & 0 & a^5_{zb} \\ a^1_{zb} & a^2_{zb} & a^3_{zb} & a^4_{zb} & 0 \\ a^1_{yb} & a^2_{yb} & a^3_{yb} & a^4_{yb} & a^5_{xb} \end{bmatrix}$$

where $a^i_{xb}, a^i_{yb}, a^i_{zb}$ are the coordinate position of ith propulsive propeller in BRF, respectively. Other detailed designed parameters of the HAA are adopted in [25].

The position $\mathbf{P}$, attitude $\boldsymbol{\Omega}$, velocity $\mathbf{v}$, and angular velocity $\boldsymbol{\omega}$ are measured by an integrated navigation system. The mearsurement noise $\boldsymbol{d}$ is added with Gaussian noise with variation of $0.01m/s^2$ to the accelerometer and $2deg/h$ to the gyro. The output matrix $\boldsymbol{C} = \boldsymbol{I}$. The unknown distrubance and system uncertainty $\boldsymbol{\eta} = \begin{bmatrix} \mathbf{0} \\ \boldsymbol{\eta}_d \end{bmatrix}$ consists of unknown input $\boldsymbol{\eta}_d = \begin{bmatrix} 20\sin(2\pi t/200) \\ 10\cos(2\pi t/190) \\ 5\sin(2\pi t/200) \\ 50\cos(2\pi t/120) \\ 50\sin(2\pi t/150) \\ 500\cos(2\pi t/170) \end{bmatrix}$.

The simulation system runs $t = 1800s$ total. The initial state $\mathbf{P}(0) = [0, 0, -18300]^T$, $\boldsymbol{\Omega}(0) = [0, 0, 0]^T$, $\mathbf{v}(0) = [0, 0, 0]^T$, and $\boldsymbol{\omega}(0) = [0, 0, 0]^T$. The HAA is expected to follow the predetermined path from [0, 0] to [40000, 7000] with expected forward velocity $u_d = 20m/s$ and pitch angle $\theta_d = 0$ in the wind $\boldsymbol{v}_w$, which is the resultant wind $\boldsymbol{v}_w = \begin{bmatrix} 2\sin(2\pi t/90) \\ -2\cos(2\pi t/110) \\ 0.5\sin(2\pi t/70) \end{bmatrix} (m/s)$ described in IRF. To ensure the HAA follows the control expectation, guidance law outputs the expected yaw ψ_d, and the propeller rotaional speed is adjusted to track. Under fault-free condition, the path tracking control result is shown in Figure 2, which gives the yaw, pitch, and forward velocity control result. Affected by wind $\boldsymbol{v}_w$ and disturbances $\boldsymbol{\eta}$, the actual trajectory, yaw ψ, pitch θ, and forward velocity u fluctuate and converge to the control expectation.

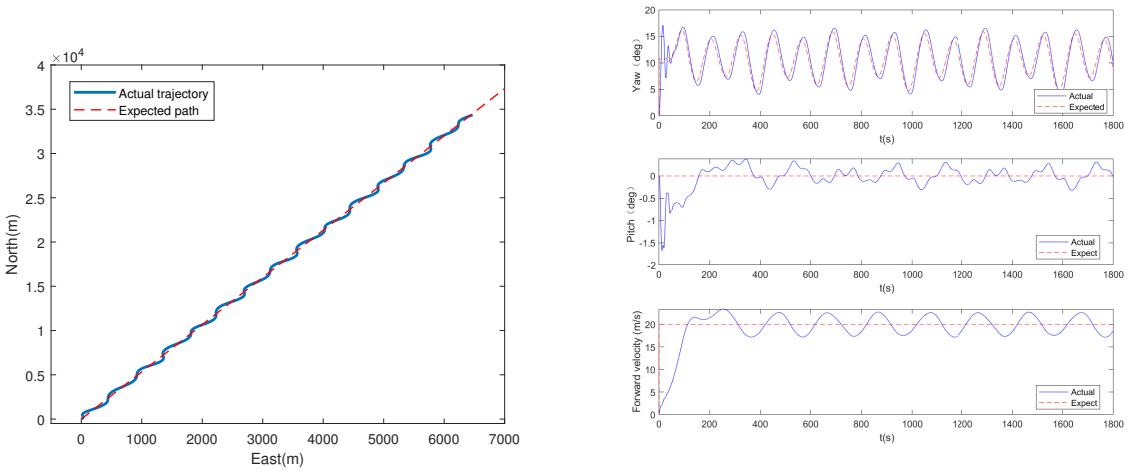

(a) The path tracking result.

(b) The attitude & velocity control result.

Figure 2. Control result of HAA path tracking without fault.

Three typical fault cases that occur in different actuator components are considered and given by:

- Case 1: $\begin{cases} \boldsymbol{f}_{a,5} = 0(N), & t \le T_d \\ \boldsymbol{f}_{a,5} = -150(N), & t > T_d \end{cases}$.
- Case 2: $\begin{cases} \rho_2(t) = 1, & t \le T_d \\ \rho_2(t) = 0.6(1 - e^{-(t-Td)}), & t > T_d \end{cases}$
- Case 3: $\begin{cases} \boldsymbol{f}_{a,3} = 0(N), \rho_3(t) = 1, & t \le T_d \\ \boldsymbol{f}_{a,3} = -80(N), \rho_2(t) = 0.5(1 - e^{-(t-Td)}), & t > T_d \end{cases}$.

where T_d denotes the time of fault occurence and is set as $T_d = 1200$s.

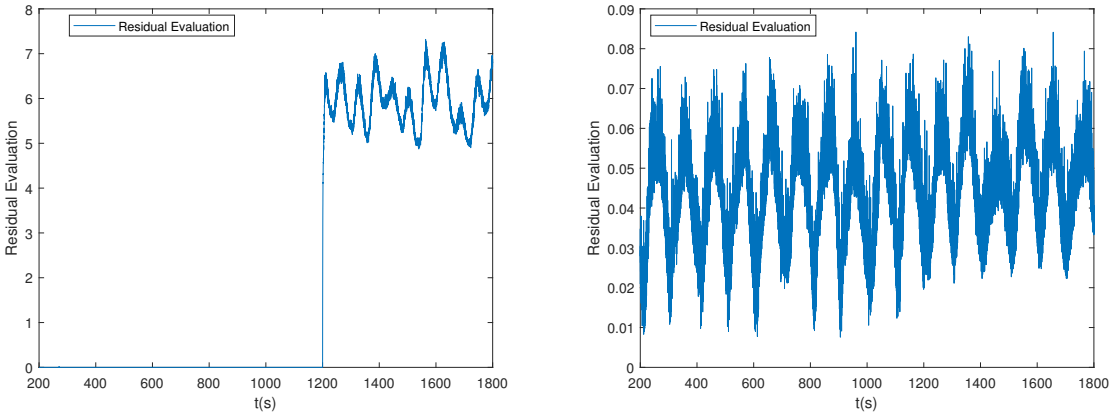

(a) Residual evaluation with proposed.

(b) Residual evaluation with $\|\boldsymbol{e}_y\|^2$.

Figure 3. Fault detection result for Case 1.

Case 1 denotes an additivity-type fault, and the invariant fault input (-150)N is added from T_d to

Propeller 5. The fault detection result is given in Figure 3 via observer (3.1). From T_d, the residulal evaluation $\|\chi_D\|^2 > 0$ gives a fault occurrent alarm as desired. Figure 3(a) shows the fault detection result accurately with proposed residual evaluation. Figure 3(b) shows the fault detection result, which cannot give the fault alarm clearly with the L_2 norm of output error $\boldsymbol{e}_y$.

There are $q = 5$ fault isolation observers obtained as (3.13), and the result is given in Figure 4. Only the residual evaluation $\|\chi_I^5\|^2 = 0$ (Figure 4(e)), not other residulal evaluations $\|\chi_I^i\|^2 > 1 (i \neq 5)$ holds from T_d. Based on the fault isolate described in Section 3.2, observer 5 decouples the affect of corresponding faulty components. Hence, the result is matched as the fault case, which is preset in Propeller 5. In Figure 4, the residual evaluation proposed in this paper can give the fault isolate result clearly. Compared to Figure 4, as shown in Figure 5(a)–(d), curves of the residual evaluation with $\|\boldsymbol{e}_y\|$ is changed from fault time T_d. However, they do not hold, exceeding the upper bound threshold, which means that it cannot give the correct fault isolation results from observers. In Figure 5(e), residual evaluation with $\|\boldsymbol{e}_y\|$ is unchanged due to the corresponding observer decoupling the faulty input effect. Residual evaluation of observers 1 to 4 have not exceeded the threshold value to present that Propeller 5 has some faulty input.

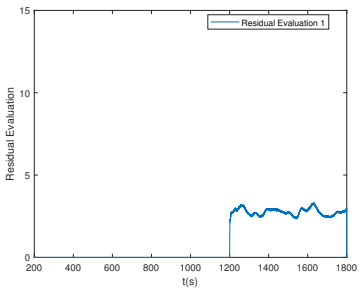

(a) Residual evaluation of fault isolate observer 1.

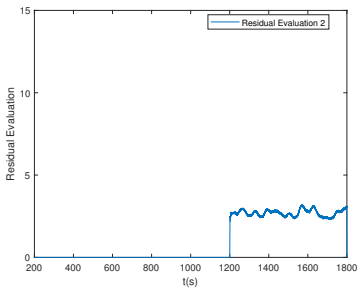

(b) Residual evaluation of fault isolate observer 2.

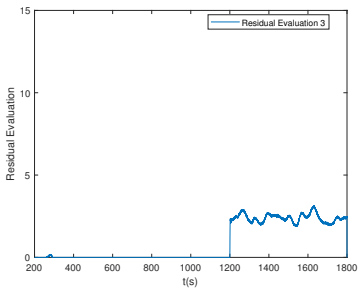

(c) Residual evaluation of fault isolate observer 3.

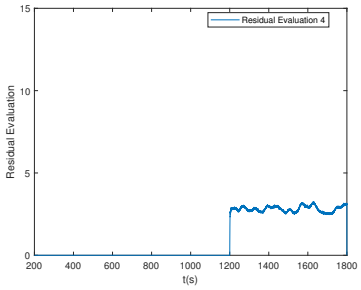

(d) Residual evaluation of fault isolate observer 4.

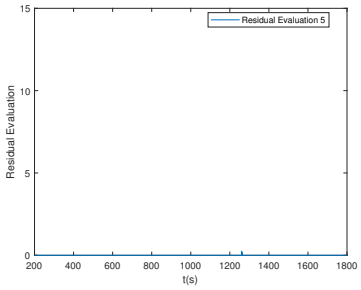

(e) Residual evaluation of fault isolate observer 5.

Figure 4. Fault isolate result with proposed residual evaluation for Case 1.

According to the result of fault isolation, the fault distribution matrix is obtained as $\boldsymbol{D} = \boldsymbol{B}_5$ to obtain observer (3.22). The result of fault reconstruction is show in Figure 6(a). The reconstructed fault is convergent to the preset fault input (-150)N. In Figure 6(b), the sum of inferred thrust and fault estimation (red dashed line denotes) is convergent to the actual thrust (blue solid line) of Propeller 5.

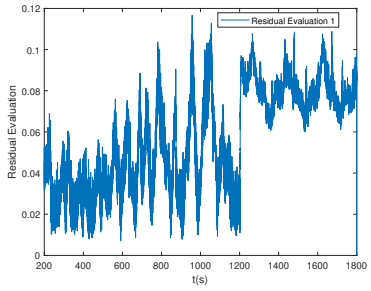

(a) Residual evaluation of fault isolate observer 1.

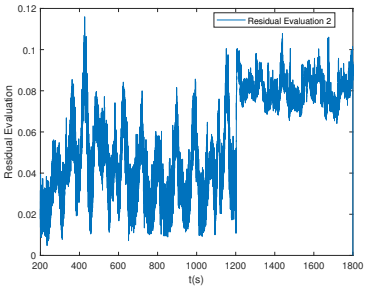

(b) Residual evaluation of fault isolate observer 2.

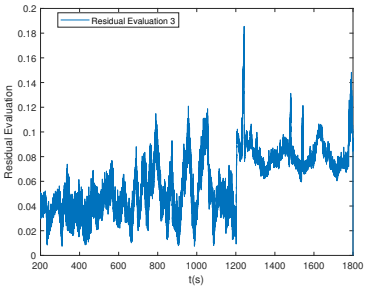

(c) Residual evaluation of fault isolate observer 3.

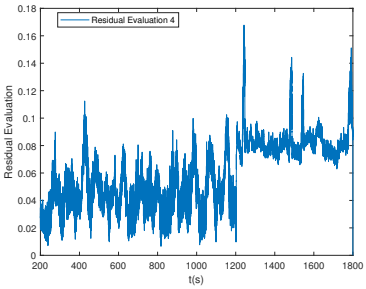

(d) Residual evaluation of fault isolate observer 4.

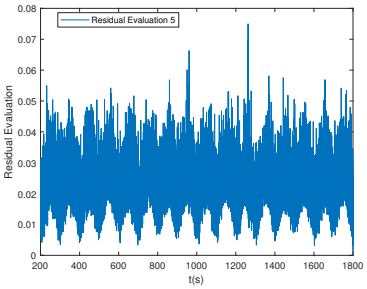

(e) Residual evaluation of fault isolate observer 5.

Figure 5. Fault isolate result with residual evaluation $\|\boldsymbol{e}_y\|^2$ for Case 1.

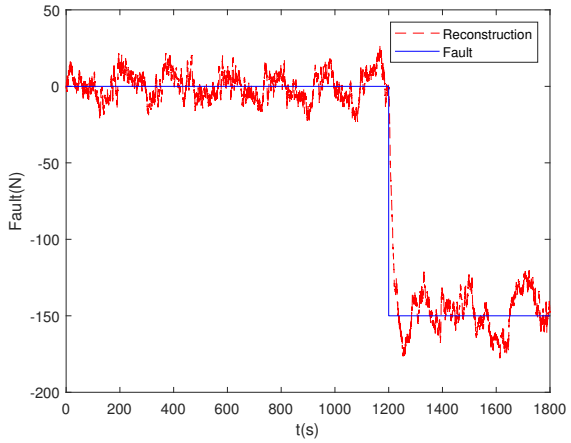

(a) Fault reconstruction.

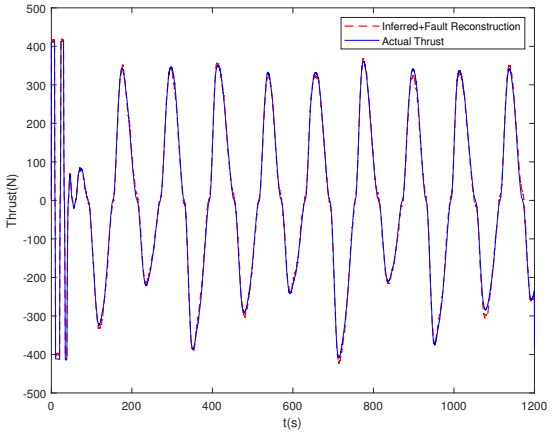

(b) Fault reconstruction.

Figure 6. Fault reconstruction result of Case 1.

Figure 7 shows the result of the sliding mode observer with Case 1. Figure 7(a) shows the curve of $\|\boldsymbol{e}_y\|^2$ in fault detection, and the residual evaluation of $\|\boldsymbol{e}_y\|^2$ has no evident changes after fault occurrence. However, compared to the fault reconstruction result with the proposed method as shown

in Figure 6(b) , the result with the sliding model observer cannot give an acceptable estimation of the unknown fault as shown as Figure 7(b).

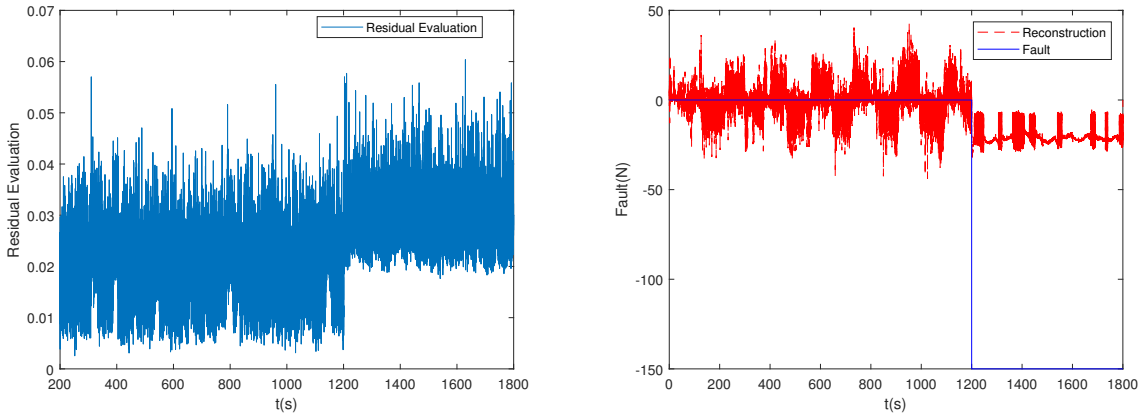

(a) Residual evaluation with $\|\boldsymbol{e}_y\|^2$.

(b) Fault reconstruction.

Figure 7. The FD result with the sliding mode observer for Case 1.

Case 2 is a multiplicative type fault where the output efficiency of Propeller 2 is down to 60% from T_d. The fault input presents time-varing and is detected with residual evaluation $\|\boldsymbol{\chi}_D\|^2 > 0$ as shown in Figure 8(a). In Figure 8(b), the fault alarm by residual evaluation is given with $\|\boldsymbol{e}_y\|^2$. The fault isolate result is given by Figure 9. The residual evaluation of observer 2 is $\|\boldsymbol{\chi}_I^2\|^2 = 0$, but for others is $\|\boldsymbol{\chi}_I^i\|^2 > 1 (i \neq 2)$. The faulty actuator is inferred to be Propeller 2. However, as shown in Figure 10, the residual evaluation in Figure 10(a),(c),(d) do not reflect the variation of fault input from T_d; only the fault isolation observer 5 senses the fault as shown in Figure 10(e). The fauty component cannot be isolated with the residual evaluation of $\|\boldsymbol{e}_y\|^2$.

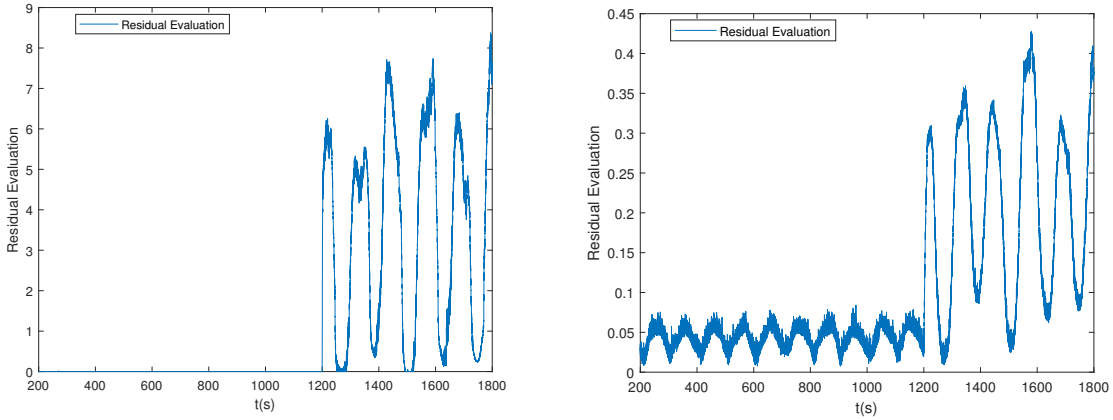

(a) Residual evaluation with proposed.

(b) Residual evaluation with $\|\boldsymbol{e}_y\|^2$.

Figure 8. Fault detection result for Case 2.

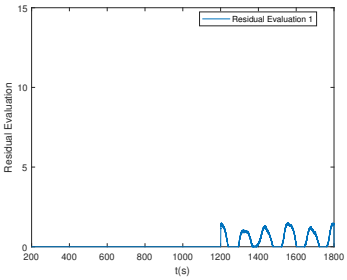

(a) Residual evaluation of fault isolate observer 1.

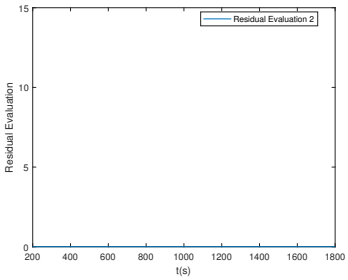

(b) Residual evaluation of fault isolate observer 2.

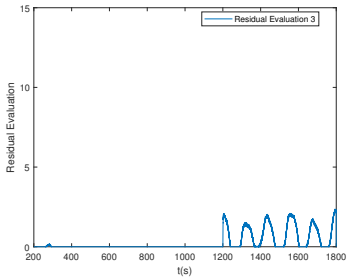

(c) Residual evaluation of fault isolate observer 3.

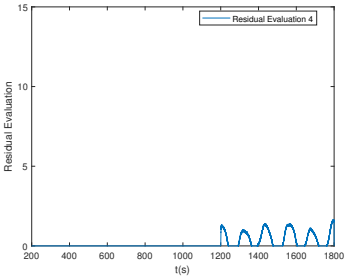

(d) Residual evaluation of fault isolate observer 4.

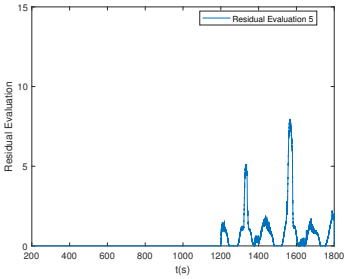

(e) Residual evaluation of fault isolate observer 5.

Figure 9. Fault isolate result with proposed residual evaluation for Case 2.

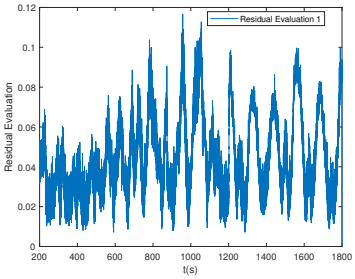

(a) Residual evaluation of fault isolate observer 1.

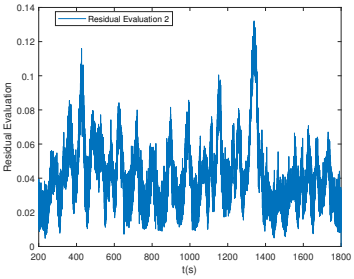

(b) Residual evaluation of fault isolate observer 2.

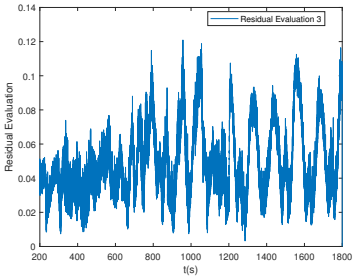

(c) Residual evaluation of fault isolate observer 3.

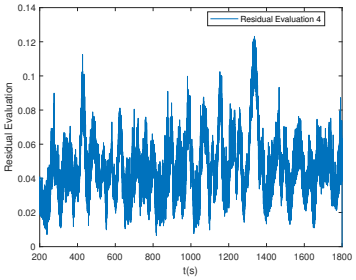

(d) Residual evaluation of fault isolate observer 4.

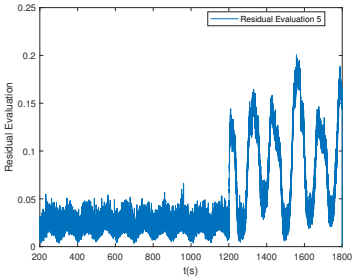

(e) Residual evaluation of fault isolate observer 5.

Figure 10. Fault isolate result with residual evaluation $||\boldsymbol{e}_y||^2$ for Case 2.

Observer (3.22) is obtained to reconstruct a fault with $\boldsymbol{D} = \boldsymbol{B}_2$, which is given in Figure 11(a). The fault reconstruct can track changes in the timing of the failure. Figure 11(b) shows that the sum of the inferred thrust and fault estimation (red dashed line denotes) is convergent to the actual thrust (blue solid line).

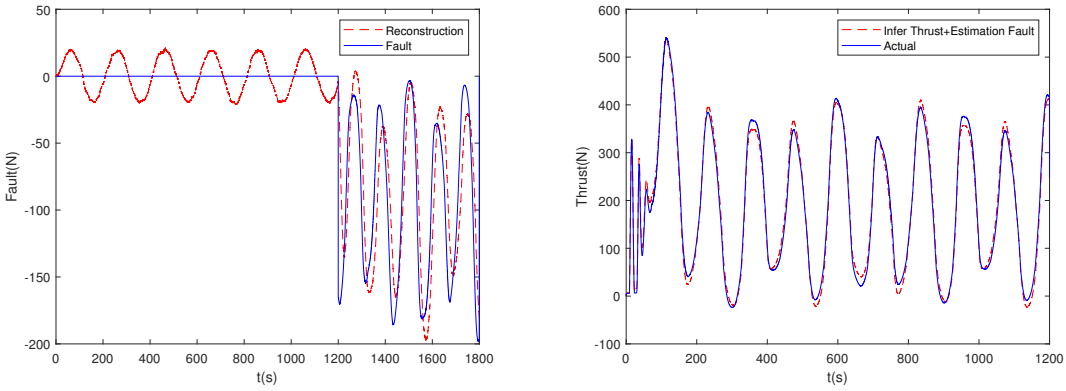

(a) Fault reconstruction. **(b)** Fault reconstruction.

Figure 11. Fault reconstruction result of Case 2.

Figure 12 shows the result of the sliding mode observer with Case 2. Figure 12(a) gives the curve of $\|\boldsymbol{e}_y\|^2$ in fault detection, and there is a noticeable change of the residual evaluation $\|\boldsymbol{e}_y\|^2$ after fault occurrence. However, compared to the fault reconstruction result with the proposed method shown in Figure 11(b), the estimation result with the sliding model observer cannot converge to the unknown fault, as shown as Figure 12(b).

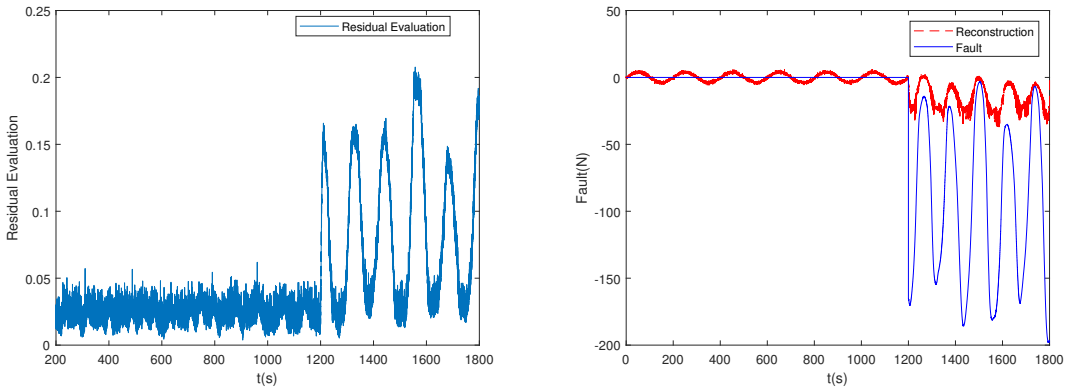

(a) Residual evaluation with $\|\boldsymbol{e}_y\|^2$. **(b)** Fault reconstruction.

Figure 12. The FD result with the sliding mode observer for Case 2.

In Case 3, the synthesizing type fault, which consists of addition and multiplication, occurs in Propeller 3 from T_d. The output efficiency is degreed to 50% and (-80)N is added. The fault detection result is shown in Figure 13. The fault detection result is more clearly with the proposed residual

evaluation method in Figure 13(a). The faulty actuator is isolated availably as shown in Figure 14. The Propeller 3 is faulty with only the residual evaluation of observer 3 holding 0. Moreover, as shown in Figure 15(a) and Figure 15(c), the residual evaluation result is indistinguishable due to the $\|\boldsymbol{e}_y\|^2$ is chosen as the residual evaluation. The residual evaluation result indicates that the corresponding actuator is faultless as shown in Figure 15(b),(d),(e). Hence, the fault cannot be isolated accurately by the residual evaluation $\|\boldsymbol{e}_y\|^2$.

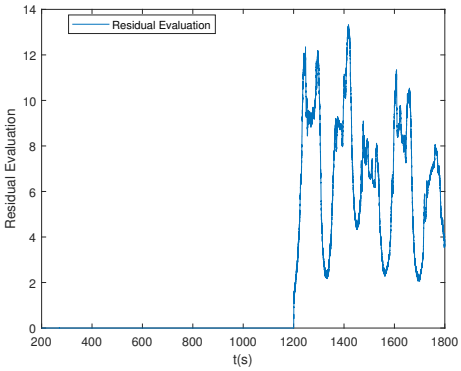

(a) Residual evaluation with proposed.

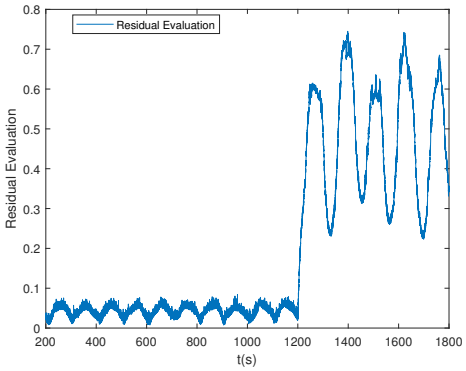

(b) Residual evaluation with $\|\boldsymbol{e}_y\|^2$.

Figure 13. Fault detection result for Case 3.

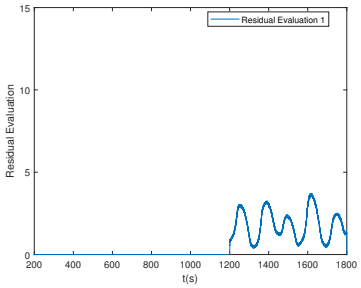

(a) Residual evaluation of fault isolate observer 1.

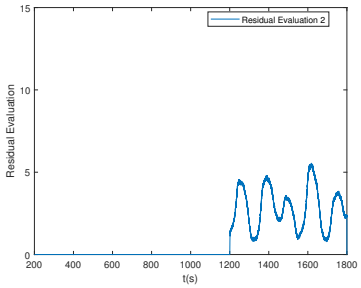

(b) Residual evaluation of fault isolate observer 2.

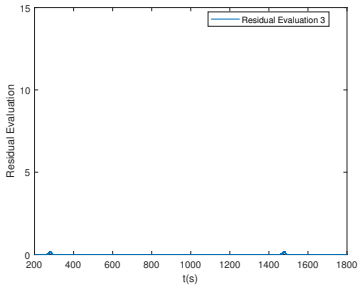

(c) Residual evaluation of fault isolate observer 3.

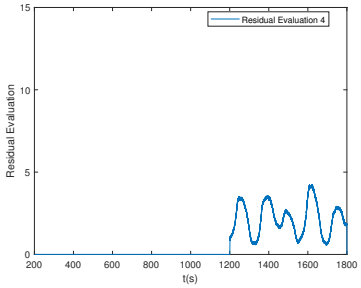

(d) Residual evaluation of fault isolate observer 4.

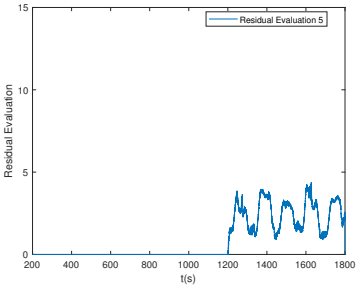

(e) Residual evaluation of fault isolate observer 5.

Figure 14. Fault isolate result with proposed residual evaluation for Case 3.

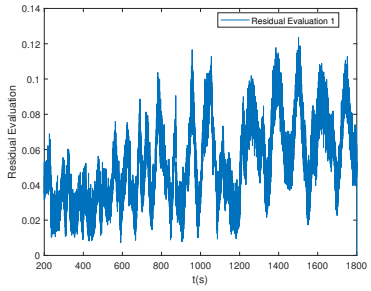

(a) Residual evaluation of fault isolate observer 1.

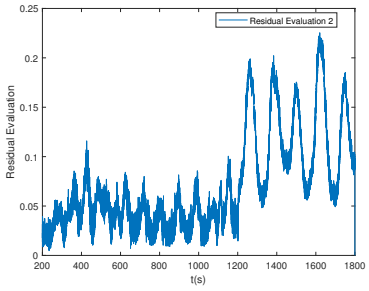

(b) Residual evaluation of fault isolate observer 2.

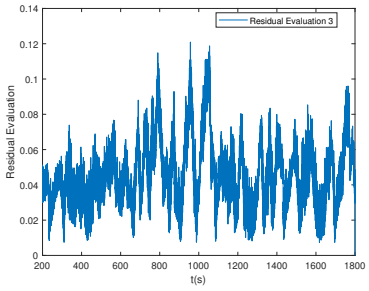

(c) Residual evaluation of fault isolate observer 3.

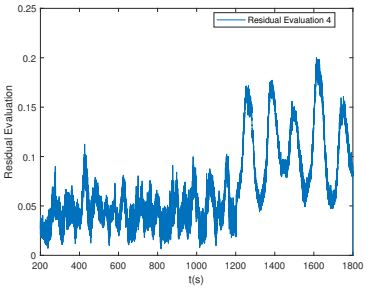

(d) Residual evaluation of fault isolate observer 4.

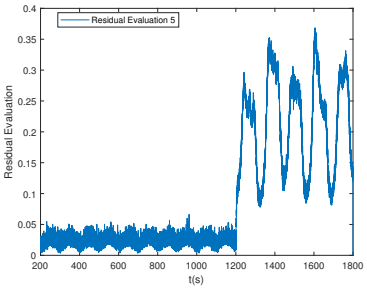

(e) Residual evaluation of fault isolate observer 5.

Figure 15. Fault isolate result with residual evaluation $\|\boldsymbol{e}_y\|^2$ for Case 3.

The result of fault reconstruction is show in Figure 16(a). The reconstructed fault is convergent to the preset time-varying fault input. In Figure 16(b), the sum of inferred thrust and fault estimation (red dashed line denotes) is convergent to the actual thrust (blue solid line).

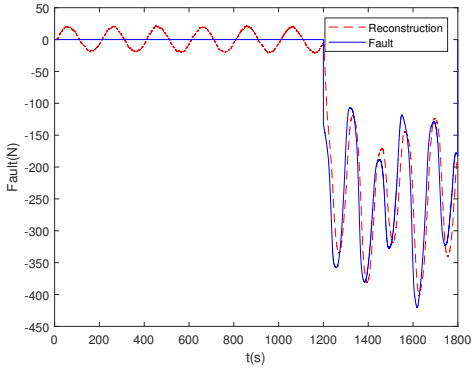

(a) Fault reconstruction

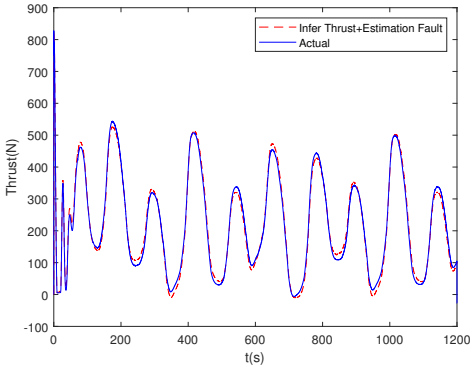

(b) Fault reconstruction

Figure 16. Fault reconstruction result of Case 3.

Figure 17 shows the result of the sliding mode observer with case 3. Figure 17(a) shows the curve of $\|\boldsymbol{e}_y\|^2$ in fault detection, and there is noticeable change of the residual evaluation of $\|\boldsymbol{e}_y\|^2$, giving the

fault alarm. However, compared to the fault reconstruction result with the proposed method as shown in Figure 16(b), the result with the sliding model observer cannot converge to the unknown fault as shown as Figure 17(b). The sliding model observer, which is applied to other nonlinear systems, is an unapplicable FD method for the HAA.

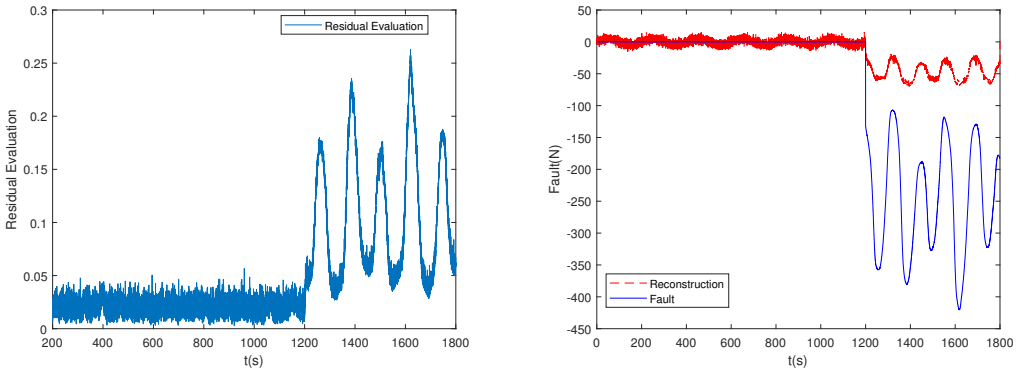

(a) Residual evaluation with $\|\boldsymbol{e}_y\|^2$. **(b)** Fault reconstruction.

Figure 17. The FD result with the sliding mode observer for Case 3.

Remark 1. *The nonlinear portion in the HAA system is continuous nonlinear, and the reformulation based on the Lipschitz property, which applies continuity, is well known. It takes all the properties of the nonlinearities of the HAA system into account.*

Remark 2. *The L_2 norm of output error $\boldsymbol{e}_y$ is empolyed as the residual and a scalar $J_{th} = \sigma \|\boldsymbol{\nu}\|^2 + \mu$ as the threshold, generally. The accuracy of the fault alarm relies on an appropriate value of μ. The proposed method does not need to consider the selection of parameter μ to get the threshold.*

Remark 3. *The scalars of measurement disturbance noise are different in various dimensions. The system output in various dimensions are normalized by the proposed method to avoid the drawback of different scalars.*

5. Conclusions

In this paper, a compositive FD method based on the nonlinear observer for the HAA is developed. Observers with different functions are obtained according to the different task demands of FD, and their existence is provided by sufficient conditions via LMIs. The error dynamic is reformulated to the LPV forms mathematically. To analyze the fault information, a developed residual evaluation is proposed. Various fault simulation cases of the HAA have been presented to show the applicability of these observers. The extension of this work to the FD method for multiple faults diagnosis is under study.

Use of AI tools declaration

The authors declare they have not used Artificial Intelligence (AI) tools in the creation of this article.

Acknowledgments

This work was supported by the National Natural Science Foundation of China (Grant No. 52402509).

Conflict of interest

The authors declare there is no conflicts of interest.

References

1. Z. Zuo, J. Song, Z. Zheng, Q. Han, A survey on modelling, control and challenges of stratospheric airships, *Control Eng. Pract.*, **119** (2022), 104979. https://doi.org/10.1016/j.conengprac.2021.104979
2. T. Chen, M. Zhu, Z. Zheng, Asymmetric error-constrained path-following control of a stratospheric airship with disturbances and actuator saturation, *Mech. Syst. Signal Process.*, **119** (2019), 501–522. https://doi.org/10.1016/j.ymssp.2018.10.003
3. J. Yuan, M. Zhu, X. Guo, W. Lou, Finite-time trajectory tracking control for a stratospheric airship with full-state constraint and disturbances, *J. Franklin Inst.*, **358** (2021), 1499–1528. https://doi.org/10.1016/j.jfranklin.2020.12.010
4. J. Yuan, X. Guo, Z. Zheng, M. Zhu, H. Gou, Error-constrained fixed-time trajectory tracking control for a stratospheric airship with disturbances, *Aerosp. Sci. Technol.*, **118** (2021), 107055. https://doi.org/10.1016/j.ast.2021.107055
5. S. Liang, S. Zhang, Y. Huang, X. Zheng, J. Cheng, S. Wu, Data-driven fault diagnosis of FW-UAVs with consideration of multiple operation conditions, *ISA Trans.*, **126** (2022), 472–485. https://doi.org/10.1016/j.isatra.2021.07.043
6. T. Thanaraj, K. H. Low, B. F. Ng, Actuator fault detection and isolation on multi-rotor UAV using extreme learning neuro-fuzzy systems, *ISA Trans.*, **138** (2023), 168–185. https://doi.org/10.1016/j.isatra.2023.02.026
7. J. J. Gertler, M. M. Kunwer, Optimal residual decoupling for robust fault diagnosis, *Int. J. Control*, **61** (1995), 395–421. https://doi.org/10.1080/00207179508921908
8. A. Khan, W. Xie, B. Zhang, L. Liu, A survey of interval observers design methods and implementation for uncertain systems, *J. Franklin Inst.*, **358** (2021), 3077–3126. https://doi.org/10.1016/j.jfranklin.2021.01.041
9. S. Meng, F. Meng, F. Zhang, Q. Li, Y. Zhang, A. Zemouche, Observer design method for nonlinear generalized systems with nonlinear algebraic constraints with applications, *Automatica*, **162** (2024), 111512. https://doi.org/10.1016/j.automatica.2024.111512
10. F. Nemati, S. M. S. Hamami, A. Zemouche, A nonlinear observer-based approach to fault detection, isolation and estimation for satellite formation flight application, *Automatica*, **107** (2019), 474–482. https://doi.org/10.1016/j.automatica.2019.06.007

11. G. Zogopoulos-Papaliakos, K. J. Kyriakopoulos, An efficient approach for graph-based fault diagnosis in UAVs, *J. Intell. Rob. Syst.*, **97** (2020), 553–576. https://doi.org/10.1007/s10846-019-01061-7
12. R. Falcón, H. Ríos, A. Dzul, A robust fault diagnosis for quad-rotors: A sliding-mode observer approach, *IEEE/ASME Trans. Mechatron.*, **27** (2022), 4487–4496. https://doi.org/10.1109/TMECH.2022.3156854
13. L. Shang, G. Liu, Sensor and actuator fault detection and isolation for a high performance aircraft engine bleed air temperature control system, *IEEE Trans. Control Syst. Technol.*, **19** (2011), 1260–1268. https://doi.org/10.1109/TCST.2010.2076353
14. Y. Wei, J. Qiu, P. Shi, L. Wu, A piecewise-markovian lyapunov approach to reliable output feedback control for fuzzy-affine systems with time-delays and actuator faults, *IEEE Trans. Cybern.*, **48** (2018), 2723–2735. https://doi.org/10.1109/TCYB.2017.2749239
15. S. Li, H. Wang, A. Aitouche, Y. Tian, N. Christov, Actuator fault and disturbance estimation using the T-S fuzzy model, *IFAC-PapersOnLine*, **50** (2017), 15722–15727. https://doi.org/10.1016/j.ifacol.2017.08.2414
16. H. Ma, Y. Liu, T. Li, G. Yang, Nonlinear high-gain observer-based diagnosis and compensation for actuator and sensor faults in a quadrotor unmanned aerial vehicle, *IEEE Trans. Ind. Inf.*, **15** (2019), 550–562. https://doi.org/10.1109/TII.2018.2865522
17. R. C. Avram, X. Zhang, J. Muse, Quadrotor actuator fault diagnosis and accommodation using nonlinear adaptive estimators, *IEEE Trans. Control Syst. Technol.*, **25** (2017), 2219–2226. https://doi.org/10.1109/TCST.2016.2640941
18. W. Chua, J. C. L. Chan, C. P. Tan, E. K. P. Chong, S. Saha, Robust fault reconstruction for a class of nonlinear systems, *Automatica*, **113** (2020), 108718. https://doi.org/10.1016/j.automatica.2019.108718
19. F. Zhu, Y. Tang, Z. Wang, Interval-observer-based fault detection and isolation design for T-S fuzzy system based on zonotope analysis, *IEEE Trans. Fuzzy Syst.*, **30** (2022), 945–955. https://doi.org/10.1109/TFUZZ.2021.3050854
20. M. Zhang, Z. Wang, Y. Wang, J. H. Park, Z. Ji, Interval observer filtering-based fault diagnosis method for linear discrete-time systems with dual uncertainties, *J. Franklin Inst.*, **359** (2022), 1626–1648. https://doi.org/10.1016/j.jfranklin.2021.11.018
21. S. Li, H. Wang, A. Aitouche, N. Christov, Sliding mode observer design for fault and disturbance estimation using takagi-sugeno model, *Eur. J. Control*, **44** (2018), 114–122. https://doi.org/10.1016/j.ejcon.2018.09.006
22. A. N. Zhirabok, A. E. Shumsky, A. V. Zuev, Fault diagnosis in linear systems via sliding mode observers, *Int. J. control*, **94** (2021), 327–335. https://doi.org/10.1080/00207179.2019.1590738
23. R. Zhou, J. Li, Z. Yang, Y. Xu, Z. Yu, Y. Zhang, Fractional-order sliding-mode fault-tolerant control of unmanned airship against actuator faults, *IFAC-PapersOnLine*, **55** (2022), 617–622. https://doi.org/10.1016/j.ifacol.2022.07.196

24. H. Hamdi, M. Rodrigues, C. Mechmeche, N. B. Braiek, Fault diagnosis based on sliding mode observer for LPV descriptor systems, *Asian J. Control*, **21** (2019), 89–98. https://doi.org/10.1002/asjc.2022

25. T. Chen, M. Zhu, Z. Zheng, Adaptive path following control of a stratospheric airship with full-state constraint and actuator saturation, *Aerosp. Sci. Technol.*, **95** (2019), 105457. https://doi.org/10.1016/j.ast.2019.105457

AIMS Press